

Torus Probabilistic Principal Component Analysis

Anahita Nodehi^{1,2,†}, Mousa Golalizadeh^{1,2,†}, Mehdi Maadooliat³, Claudio Agostinelli⁴

¹*Department of Statistics, Tarbiat Modares University, Tehran, Iran*

²*School of Biological Science, Institute for Research in Fundamental Sciences (IPM), Tehran, Iran*

³*Department of Mathematical and Statistical Sciences, Marquette University, Milwaukee, USA*

⁴*Department of Mathematics, University of Trento, Trento, Italy*

Abstract

Analyzing data in non-Euclidean spaces, such as bioinformatics, biology, and geology, where variables represent directions or angles, poses unique challenges. This type of data is known as circular data in univariate cases and can be termed spherical or toroidal in multivariate contexts. In this paper, we introduce a novel extension of Probabilistic Principal Component Analysis (PPCA) designed for toroidal (or torus) data, termed Torus Probabilistic PCA (TPPCA). We provide detailed algorithms for implementing TPPCA and demonstrate its applicability to torus data. To assess the efficacy of TPPCA, we perform comparative analyses using a simulation study and three real datasets. Our findings highlight the advantages and limitations of TPPCA in handling torus data. Furthermore, we propose statistical tests

[†]**Corresponding author:** Anahita Nodehi & Mousa Golalizadeh, Department of Statistics, Tarbiat Modares University, Tehran, Iran. Email: ana.nodehi@yahoo.com - golalizadeh@modares.ac.ir.

⁰**Mathematics Subject Classification (2020):** 62Hxx, 62H25, 62H11.

based on likelihood ratio statistics to determine the optimal number of components, enhancing the practical utility of TPPCA for real-world applications.

Keywords: Probabilistic Principal Component Analysis; Non-Euclidean Space; Torus Data; Wrapped Normal distribution.

1 Introduction

Angular data, characterized by a large number of variables, presents significant challenges when applying statistical methods. These challenges include difficulties in data visualization, increased computational demands, and a higher risk of over- or under-fitting during modeling. To address these issues, dimension reduction methods are commonly employed. Principal Component Analysis (PCA) is a well-known technique in classical Euclidean space, with origins dating back to Pearson [1901] and Hotelling [1933]. The main idea of PCA is to reduce the dimensionality of a data set by uncorrelated components, retaining as much of the variation present in the data set as possible [Jolliffe, 2002]. The PCA is also one of the main tools extracting information from large datasets in bioinformatics; to name a few, we can mention problems in genetics [Price et al., 2006, Novembre and Stephens, 2008, Privé et al., 2020], in meta-analysis [Kim et al., 2018] and shape analysis [Wiseman et al., 2021, Moghimbeygi and Nodehi, 2022]. Classic PCA lacks a probabilistic framework and associated likelihood measures, which can limit specific applications. A probabilistic formulation is often preferred because of its capacity to enable comparisons with other probabilistic techniques, facilitate statistical testing, and support the application of Bayesian methods. It also improves the handling of missing data [Tipping and Bishop, 1997]. Probabilistic PCA (PPCA) is an extension of PCA, offering a maximum likelihood solution within a probabilistic latent variable model. PPCA was independently introduced by Tipping and Bishop [1997, 1999] and Roweis [1998] and is closely related to factor analysis [Basilevsky, 1994].

There are numerous situations in applied sciences, such as biology, bioinformatics, astronomy, and geology, where the data are supported in non-Euclidean spaces. For example, wind directions (in meteorology), animal navigation (in biology), and the epicenter of an earthquake (in earth sciences) are three classical instances of direction measurements in applied sciences.

It is common to specify a measure as an angle on a unit circle once the circle’s initial direction and orientation have been chosen. In bioinformatics, angles are the suitable components to represent the protein structure. In detail, there are two torsional angles (ϕ, ψ) in the protein backbones for each amino acid residue [Maadooliat et al., 2016]. In RNA, the dimensionality is much more complex. For each nucleotide residue, there are seven independent torsion angles and one angle that describes the rotation of the base relative to the sugar [Eltzner et al., 2018]. The statistical analysis of such angular data is known as directional statistics [Mardia, 1972]. Some authors named directional data as “circular data” and “angular data” in univariate cases and “spherical data” or “torus data” in multivariate cases. Accordingly, these data types are also part of the so-called “non-Euclidean data” or “manifold-valued data”. There have been many attempts to extend PCA on manifold data. To name a few: Principal Curve [Hastie and Stuetzle, 1989], Principal Geodesic Analysis (PGA) [Fletcher et al., 2004], Geodesic Principal Component Analysis (GPCA) [Huckemann and Ziezold, 2006], dihedral angles Principal Component Analysis (dPCA) (Mu et al. [2005] and Altis et al. [2007]), and angular PCA (aPCA) [Riccardi et al., 2009], Principal Arc Analysis (PAA) [Jung et al., 2010], Principal Nested Analysis (PNS) [Jung et al., 2012], Principal Geodesic Analysis on the shape space [Fotouhi and Golarizadeh, 2012, 2015], Principal Flows (PF) [Panaretos et al., 2014], dihedral angles Principal Geodesic Analysis [Nodehi et al., 2015], PCA on torus (dPCA+) [Sittel et al., 2017], Torus Principal Component Analysis (T-PCA) [Eltzner et al., 2018] and Scaled Torus PCA (ST-PCA) [Zoubouoglou et al., 2022].

In the literature exploring torus-specific PCA techniques for analyzing toroidal data, we explore modern methods designed for practical application. The dPCA, introduced by Mu et al. [2005] and Altis et al. [2007], transforms dihedral angles into sinusoidal and cosinusoidal representations. Furthermore, angular PCA (aPCA) and Cartesian PCA (cPCA) apply PCA to torus data, centered on their circular means [Riccardi et al., 2009]. Altis et al. [2007] proposes Complex dPCA as an alternative extension to the sin/cos transformation in dPCA, transforming angles into complex numbers using Euler’s formula. Further advancements include dihedral angles Principal Geodesic Analysis [Nodehi et al., 2015], which is an extension of PGA to dihedral angles in protein structures. The PCA on the torus (dPCA+) [Sittel et al., 2017] is a customized solution that minimizes projection errors in the torus data due to periodicity. Torus Principal Component Analysis

(T-PCA) by Eltzner et al. [2018] deforms tori into spheres using PNS and introduces data-adaptive pre-clustering. In addition, Eltzner et al. [2018] proposed two data-driven orderings of variables, *SI ordering* and *SO ordering*, corresponding to the order of the variables in terms of the decreasing and increasing amount of circular variability, respectively. Lastly, Scaled Torus Principal Component Analysis (ST-PCA) by Zoubouloglou et al. [2022] is a recent method based on spherical embeddings, using Spherical MultiDimensional Scaling (SMDS) to map from a torus to a sphere. In ST-PCA, the analyses are done on spheres, and after finding the best fit of data, it can be inverted back to the torus. For detailed technical information, comprehensive descriptions of these methods can be found in the Supplementary Material.

Despite advances in extending PCA methods, a significant gap remains in the application of probabilistic modeling to manifold-valued datasets, particularly in the context of torus data. While recent developments have extended PCA to non-Euclidean spaces using probabilistic approaches, such as the Probabilistic PGA for spherical data introduced by Zhang and Fletcher [2013] and the method for genotype data proposed by Agrawal et al. [2020], there is still no established probabilistic PCA framework specifically designed for toroidal data. This gap is critical, given the unique properties of toroidal manifolds that standard PCA techniques cannot adequately address. To address this need, we introduce Torus Probabilistic PCA (TPPCA), a novel extension of Probabilistic PCA designed explicitly for torus data. Our approach includes an efficient iterative algorithm that fully utilizes the unique structure of toroidal manifolds, providing a robust solution to the challenges of feature extraction in this space. TPPCA not only allows for comparisons with other probabilistic methods but also enables the application of statistical testing to determine the optimal number of components. This novel technique provides a valuable tool for analyzing toroidal data.

The remainder of this paper is organised as follows: In Section 2, we introduce the methodology of TPPCA and a discussion on the selection of the number of components. The empirical contributions of the paper are highlighted in Section 3, where we present the results of our simulation study and explore three real-world applications, demonstrating the practical implications of our proposal. Lastly, in Section 4, we present our concluding thoughts and remarks, wrapping up the key insights and contributions of the paper.

2 Torus Probabilistic Principal Component Analysis

We introduce an extension of PPCA for toroidal data. Let $X \in \mathbb{R}$ be a real random variable, a circular random variable Y might be written as $Y = X \bmod 2\pi \in [0, 2\pi)$ or $X = Y + 2\pi K$ for some $K \in \mathbb{Z}$. Let $\mathbb{T}^D = [0, 2\pi)^D$ be the D -torus. The TPPCA is a latent variable model that seeks to relate a D -dimensional observation vector $\mathbf{Y} \in \mathbb{T}^D$ to a corresponding d -dimensional vector of latent (or unobserved) variables $\mathbf{Z} \in \mathbb{R}^d$ ($d < D$), that is,

$$\begin{aligned} \mathbf{Y} &= \mathbf{X} \bmod 2\pi \\ \mathbf{X} &= \boldsymbol{\mu} + \mathbf{W}\mathbf{Z} + \boldsymbol{\epsilon}, \end{aligned} \tag{1}$$

where \mathbf{W} is a $(D \times d)$ matrix that relates the two sets of variables, $\mathbf{X} = (X_1, \dots, X_D)^\top$, $\mathbf{Z} = (Z_1, \dots, Z_d)^\top$, while the parameter vector $\boldsymbol{\mu}$ allows the model to have a non-zero mean. The vector $\mathbf{Z} \sim N_d(\mathbf{0}, \mathbf{I}_d)$ represents a d -dimensional Gaussian latent variable, and $\boldsymbol{\epsilon} \sim N_D(\mathbf{0}, \sigma^2 \mathbf{I}_D)$ is a D -dimensional zero-mean Gaussian noise variable with covariance $\sigma^2 \mathbf{I}_D$. We assume $\text{Cov}(\mathbf{Z}, \boldsymbol{\epsilon}) = \mathbf{0}$ and there exists a random vector $\mathbf{K} = \mathbf{K}(\mathbf{X})$ such that $\mathbf{Y} = \mathbf{X} - 2\pi\mathbf{K} \in \mathbb{T}^D$. We recall the following basic results [Mardia et al., 1979]

$$\begin{aligned} \mathbf{X} &\sim N_D(\boldsymbol{\mu}, \mathbf{W}\mathbf{W}^\top + \sigma^2 \mathbf{I}_D), \\ \mathbf{X}|\mathbf{Z} &\sim N_D(\boldsymbol{\mu} + \mathbf{W}\mathbf{Z}, \sigma^2 \mathbf{I}_D), \\ \mathbf{Z}|\mathbf{X} &\sim N_d(\mathbf{M}^{-1}\mathbf{W}^\top(\mathbf{X} - \boldsymbol{\mu}), \sigma^2 \mathbf{M}^{-1}), \\ \mathbf{Z}|\mathbf{Y} &\sim N_d(\mathbf{M}^{-1}\mathbf{W}^\top(\mathbf{Y} + 2\pi\mathbf{K} - \boldsymbol{\mu}), \sigma^2 \mathbf{M}^{-1}), \end{aligned} \tag{2}$$

where $\mathbf{M} = \mathbf{W}^\top \mathbf{W} + \sigma^2 \mathbf{I}_d$. For a given point $\mathbf{x} \in \mathbb{R}^D$ we define a parameter vector $\mathbf{k} \in \mathbb{Z}^D$ so that $\mathbf{y} = \mathbf{x} - 2\pi\mathbf{k} \in \mathbb{T}^D$, then

$$f(\mathbf{y}, \mathbf{x}, \mathbf{z}, \mathbf{k}) = f(\mathbf{y}, \mathbf{k}|\mathbf{x}, \mathbf{z})f(\mathbf{x}|\mathbf{z})f(\mathbf{z}) = f(\mathbf{y}, \mathbf{k}|\mathbf{x})f(\mathbf{x}|\mathbf{z})f(\mathbf{z}),$$

where

$$f(\mathbf{y}, \mathbf{k}|\mathbf{x}) = \mathbb{1}(\mathbf{y}, \mathbf{k}, \mathbf{x}) = \begin{cases} 1 & \text{if } \mathbf{y} \in \mathbb{T}^D \text{ and } \mathbf{k} = \frac{\mathbf{x} - \mathbf{y}}{2\pi} \\ 0 & \text{otherwise,} \end{cases}$$

which leads to the joint distribution

$$f(\mathbf{y}, \mathbf{x}, \mathbf{z}, \mathbf{k}) \propto \mathbb{1}(\mathbf{y}, \mathbf{x}, \mathbf{k}) (\sigma^2)^{-\frac{D}{2}} \times \exp \left\{ -\frac{(\mathbf{y} + 2\pi\mathbf{k} - \mathbf{W}\mathbf{z} - \boldsymbol{\mu})^\top (\mathbf{y} + 2\pi\mathbf{k} - \mathbf{W}\mathbf{z} - \boldsymbol{\mu})}{2\sigma^2} - \frac{\mathbf{z}^\top \mathbf{z}}{2} \right\}.$$

Let $\mathcal{Y} = (\mathbf{y}_1, \dots, \mathbf{y}_N)$ be a sample of size N and let $\mathcal{K} = (\mathbf{k}_1, \dots, \mathbf{k}_N)$ a set of missing values from the random vector \mathbf{K} , then the logarithm of the likelihood function, say $\ell(\boldsymbol{\mu}, \mathbf{W}, \sigma^2, \mathcal{K})$, is given by

$$\begin{aligned} \ell(\boldsymbol{\mu}, \mathbf{W}, \sigma^2, \mathcal{K}) &= \sum_{j=1}^N \ln f(\mathbf{y}_j, \mathbf{x}_j, \mathbf{z}_j, \mathbf{k}_j) \\ &\propto \sum_{j=1}^N \left[-\frac{D}{2} \ln \sigma^2 - \frac{(\mathbf{x}_j - \mathbf{W}\mathbf{z}_j - \boldsymbol{\mu})^\top (\mathbf{x}_j - \mathbf{W}\mathbf{z}_j - \boldsymbol{\mu})}{2\sigma^2} - \frac{\mathbf{z}_j^\top \mathbf{z}_j}{2} \right] \\ &\times \mathbb{1}(\mathbf{y}_j, \mathbf{k}_j, \mathbf{x}_j) \\ &\propto \sum_{j=1}^N \left[-D \ln \sigma^2 - \frac{\text{tr}[(\mathbf{y}_j + 2\pi\mathbf{k}_j - \boldsymbol{\mu})(\mathbf{y}_j + 2\pi\mathbf{k}_j - \boldsymbol{\mu})^\top]}{\sigma^2} \right. \\ &\left. + 2 \frac{(\mathbf{y}_j + 2\pi\mathbf{k}_j - \boldsymbol{\mu})\mathbf{z}_j^\top \mathbf{W}^\top}{\sigma^2} - \frac{\text{tr}[(\mathbf{W}\mathbf{z}_j)(\mathbf{W}\mathbf{z}_j)^\top]}{\sigma^2} - \text{tr}(\mathbf{z}_j\mathbf{z}_j^\top) \right] \\ &\times \mathbb{1}(\mathbf{y}_j, \mathbf{k}_j, \mathbf{x}_j), \end{aligned}$$

where in the last line we use the fact $\text{tr}(\mathbf{AB}) = \text{tr}(\mathbf{BA})$. We are going to take expectation of the log-likelihood over the latent variables $\mathbf{Z}_1, \dots, \mathbf{Z}_N$

given the data sample \mathcal{Y} , that is,

$$\begin{aligned}
\Gamma(\boldsymbol{\mu}, \mathbf{W}, \sigma^2, \mathcal{K}|\mathcal{Y}) &= \mathbb{E}(\ell|\mathcal{Y}) = \sum_{j=1}^N \mathbb{E}(\ell(\boldsymbol{\mu}, \mathbf{W}, \sigma^2, \mathcal{K})|\mathbf{Y}_j = \mathbf{y}_j) \\
&\propto \sum_{j=1}^N \left\{ -D \ln \sigma^2 - \text{tr}[\mathbb{E}(\mathbf{Z}_j \mathbf{Z}_j^\top | \mathbf{Y}_j = \mathbf{y}_j)] \right. \\
&\quad - \frac{(\mathbf{y}_j + 2\pi \mathbf{k}_j - \boldsymbol{\mu})(\mathbf{y}_j + 2\pi \mathbf{k}_j - \boldsymbol{\mu})^\top}{\sigma^2} \\
&\quad + 2 \frac{(\mathbf{y}_j - \boldsymbol{\mu} + 2\pi \mathbf{k}_j) \mathbb{E}(\mathbf{Z}_j^\top | \mathbf{Y}_j = \mathbf{y}_j) \mathbf{W}^\top}{\sigma^2} \\
&\quad \left. - \frac{\text{tr}[\mathbf{W} \mathbb{E}(\mathbf{Z}_j \mathbf{Z}_j^\top | \mathbf{Y}_j = \mathbf{y}_j) \mathbf{W}^\top]}{\sigma^2} \right\} \\
&\times \mathbb{1}(\mathbf{y}_j, \mathbf{k}_j, \mathbf{x}_j) \\
&= \sum_{j=1}^N \left\{ -D \ln \sigma^2 - \text{tr}[\mathbb{E}(\mathbf{Z}_j \mathbf{Z}_j^\top | \mathbf{X}_j = \mathbf{y}_j + 2\pi \mathbf{k}_j)] \right. \\
&\quad - \frac{(\mathbf{y}_j + 2\pi \mathbf{k}_j - \boldsymbol{\mu})^\top (\mathbf{y}_j + 2\pi \mathbf{k}_j - \boldsymbol{\mu})}{\sigma^2} \\
&\quad - \frac{\text{tr}[\mathbf{W} \mathbb{E}(\mathbf{Z}_j \mathbf{Z}_j^\top | \mathbf{X}_j = \mathbf{y}_j + 2\pi \mathbf{k}_j) \mathbf{W}^\top]}{\sigma^2} \\
&\quad \left. + 2 \frac{(\mathbf{y}_j + 2\pi \mathbf{k}_j - \boldsymbol{\mu}) \mathbb{E}(\mathbf{Z}_j^\top | \mathbf{X}_j = \mathbf{y}_j + 2\pi \mathbf{k}_j) \mathbf{W}^\top}{\sigma^2} \right\} \\
&\times \mathbb{1}(\mathbf{y}_j, \mathbf{k}_j, \mathbf{x}_j),
\end{aligned}$$

where in the last line, given a function $g(\cdot)$ and the definition of \mathbf{k} we see that

$$\mathbb{E}(g(\mathbf{Z})|\mathbf{Y} = \mathbf{y}) = \mathbb{E}(g(\mathbf{Z})|\mathbf{X} = \mathbf{y} + 2\pi \mathbf{k}).$$

To provide an overview of TPPCA, the proposed algorithm can be summarized in one initial step (Step 0) followed by an iterative procedure consisting of two steps (Steps 1 and 2), which are repeated until convergence:

Step 0: Initial Estimates

The initial estimates for the parameters $\boldsymbol{\mu}$, \mathbf{W} , and σ^2 , as well as a reasonable imputation of \mathcal{K} , are crucial for the convergence and performance of the

proposed algorithm. Initially, an unstructured variance-covariance matrix Σ is assumed, such that $\mathbf{Y} \sim WN_D(\boldsymbol{\mu}, \Sigma)$. The initial estimates $\hat{\mathcal{K}}_0 = (\hat{\mathbf{k}}_1, \dots, \hat{\mathbf{k}}_N)$ are obtained using the Classification Expectation-Maximization (CEM) algorithm proposed by Nodehi et al. [2021]. Subsequently, a strategy similar to that used by Tipping and Bishop [1999] is employed to maximize the log-likelihood $\ell(\boldsymbol{\mu}, \mathbf{W}, \sigma^2, \hat{\mathcal{K}}_0)$ with respect to the parameters, yielding the initial estimates $(\hat{\boldsymbol{\mu}}_0, \hat{\mathbf{W}}_0, \hat{\sigma}_0^2)$. These estimates are then used to initiate the iterative algorithm (Steps 1 and 2).

Step 1: Updating $\boldsymbol{\mu}$ and \mathcal{K}

In this step, $\boldsymbol{\mu}$ is updated and the missing values of \mathcal{K} are imputed using the CEM algorithm, as described by Nodehi et al. [2021]. The CEM algorithm is iteratively applied to maximize the conditional expectation of the log-likelihood, consisting of the following steps:

- **E-step (Expectation):** Compute the expectation $\Gamma(\hat{\boldsymbol{\mu}}_{i-1}, \hat{\mathbf{W}}_{i-1}, \hat{\sigma}_{i-1}^2, \mathcal{K}|\mathcal{Y})$.
- **C-step (Classification):** Update $\hat{\mathcal{K}}_i$ by maximizing the expected complete-data log-likelihood with respect to \mathcal{K} .
- **M-step (Maximization):** Update $\hat{\boldsymbol{\mu}}_i$ by solving:

$$\hat{\boldsymbol{\mu}}_i = \frac{1}{N} \sum_{j=1}^N (\mathbf{y}_j + 2\pi \hat{\mathbf{k}}_{i,j}).$$

This process is repeated until convergence of $\hat{\boldsymbol{\mu}}_i$ and $\hat{\mathcal{K}}_i$.

Step 2: Updating \mathbf{W} and σ^2

After obtaining updated values for $\boldsymbol{\mu}$ and \mathcal{K} , the next step is to update the estimates of \mathbf{W} and σ^2 . This is accomplished by maximizing the log-likelihood function with respect to these parameters. The updated estimates are given by:

$$\hat{\mathbf{W}}_i = \hat{\mathbf{S}}_i \hat{\mathbf{W}}_{i-1} \hat{\mathbf{M}}_{i-1}^{-1} (\sigma^2 \mathbf{I}_d + \hat{\mathbf{M}}_{i-1}^{-1} \hat{\mathbf{W}}_{i-1}^\top \hat{\mathbf{S}}_i \hat{\mathbf{W}}_{i-1})^{-1},$$

where $\hat{\mathbf{S}}_i = \frac{1}{N} \sum_{j=1}^N (\hat{\mathbf{x}}_j - \hat{\boldsymbol{\mu}}_i)(\hat{\mathbf{x}}_j - \hat{\boldsymbol{\mu}}_i)^\top$ and $\hat{\mathbf{M}}_{i-1} = \hat{\mathbf{W}}_{i-1}^\top \hat{\mathbf{W}}_{i-1} + \hat{\sigma}_{i-1}^2 \mathbf{I}_d$. The estimate for σ^2 is then updated using:

$$\hat{\sigma}_i^2 = \frac{1}{D} \text{tr}[\hat{\mathbf{S}}_i(\mathbf{I} - \hat{\mathbf{W}}_i \hat{\mathbf{M}}_i^{-1} \hat{\mathbf{W}}_i^\top)],$$

where $\hat{\mathbf{M}}_i = \hat{\mathbf{W}}_i^\top \hat{\mathbf{W}}_i + \hat{\sigma}_{i-1}^2 \mathbf{I}_d$.

This iterative algorithm, which integrates the CEM algorithm in the first step, refines the estimates for $\boldsymbol{\mu}$, \mathcal{K} , \mathbf{W} , and σ^2 until convergence. Unlike the approach in Nodehi et al. [2021], which focused solely on estimating $\boldsymbol{\mu}$ and \mathcal{K} with a general covariance structure, the present work extends this by also estimating the loading matrix \mathbf{W} associated with the principal components of the wrapped normal model and σ^2 . This extension enables a more comprehensive analysis of toroidal data using TPPCA. The details of this algorithm can be found in the Supplementary Material.

Selection of the number of components

In PCA and Factor Analysis (FA), one of the key challenges is determining the optimal number of components to retain. Over the past several decades, various methods have been developed to tackle this problem. These include: **(a) proportion of variance** [Jackson, 1991] which evaluates the cumulative variance explained by each component, **(b) Kaiser-Guttman:** a criterion that involves counting the number of eigenvalues of the sample correlation matrix that exceed one, as initially proposed by Guttman [1954] and Kaiser [1960], **(c) eigenvalue-based methods:** the number of positive eigenvalues of the sample correlation matrix whose j^{th} diagonal element is replaced by the squared multiple correlations between the j^{th} variable and the rest of the $D - 1$ variables, $j = 1, \dots, D$ [Hayashi et al., 2007], **(d) Likelihood Ratio Test (LRT):** a method that employs maximum likelihood analysis to evaluate the significance of additional components [Bartlett, 1950, Jöreskog, 1967], **(e) Akaike information criterion (AIC)** [Akaike, 1987] and its variations, including CAIC [Bozdogan, 1994] and BIC [Schwarz, 1978], **(f) Cross-Validation (CV)** which is proposed by Krzanowski [1987].

Given the probabilistic nature of our model, this paper developed the use of the LRT, specifically for torus data. We explore two different LRT-based tests to assess the number of factors, both of which are conventional in covariance structure analysis [Lawley and Maxwell, 1971, Bartlett, 1950].

The first approach is the standard model goodness-of-fit test (Type 1), while the second is a Chi-square difference test (Type 2). In Factor Analysis, the Bartlett correction is generally not applied to the difference test. Therefore, we employ the Chi-square difference test (Type 2) in our analysis, taking into account the differences between PPCA and Factor Analysis. This section explores the LRT and its extension to TPPCA.

If the distribution of the random samples $\mathcal{X} = (\mathbf{X}_1, \dots, \mathbf{X}_n)^\top$ depends on a parameter vector $\boldsymbol{\theta} \in \Theta$ and if $H_0 : \boldsymbol{\theta} \in \Theta_0$ and $H_1 : \boldsymbol{\theta} \in \Theta_1 = \Theta - \Theta_0$ are related hypotheses, then the likelihood ratio statistics for testing H_0 against H_1 is defined as

$$\lambda = \frac{L_0^*}{L_1^*},$$

where L_i^* is the largest value which the likelihood function takes in region Θ_i , $i = 0, 1$. Equivalently, we might use the log-likelihood statistics

$$-2 \log \lambda = -2(l_0^* - l_1^*)$$

where $l_i^* = \log L_i^*$, $i = 0, 1$ [Mardia et al., 1979]. Thus, to perform the LRT, we have

$$\begin{aligned} l_0^* &\propto -\frac{n}{2} \log |\hat{\mathbf{C}}| - \frac{n}{2} \text{tr}(\hat{\mathbf{C}}^{-1} \mathbf{S}) \\ l_1^* &\propto -\frac{n}{2} \log |\mathbf{S}| - \frac{n}{2} \text{tr}(\mathbf{S}^{-1} \mathbf{S}) = -\frac{n}{2} \log |\mathbf{S}| - \frac{nD}{2} \end{aligned}$$

where $\hat{\mathbf{C}} = \hat{\mathbf{W}}\hat{\mathbf{W}}^\top + \hat{\sigma}^2 \mathbf{I}_D$ is an estimate of \mathbf{C} . Then the statistical test is given by

$$\begin{aligned} U_d &= -2 \log \lambda = -2 \log(L_0^* - L_1^*) \\ &= -n \log |\hat{\mathbf{C}}^{-1} \mathbf{S}| + n \text{tr}(\hat{\mathbf{C}}^{-1} \mathbf{S}) - nD \\ &= -n \log (g^D) + n(Da) - nD \\ &= nD(a - \log g - 1), \end{aligned} \tag{3}$$

where U_d is calculated based on the eigenvalues of $\hat{\mathbf{C}}^{-1} \mathbf{S}$. To clarify, let a represent the arithmetic mean and g the geometric mean of these eigenvalues. The relationship can be expressed as $\text{tr}(\hat{\mathbf{C}}^{-1} \mathbf{S}) = Da$ and $\det(\hat{\mathbf{C}}^{-1} \mathbf{S}) = g^D$. For toroidal data, we utilized the two-step iterative algorithm in TPPCA to estimate the parameters \mathbf{W} and σ^2 . With these estimates, U_d was subsequently computed as per equation (3).

Following the Chi-square difference test’s approach for testing the d -component model against the $(d + 1)$ -component model, we consider the following hypothesis

$$\begin{aligned} H_0 : \Sigma = \mathbf{C} \text{ with } \mathbf{W} \text{ is } D \times d \text{ matrix} \\ H_1 : \Sigma = \mathbf{C} \text{ with } \mathbf{W} \text{ is } D \times (d + 1) \text{ matrix.} \end{aligned}$$

It is easy to see that the LRT statistic is given by

$$V_d = U_d - U_{d+1} ,$$

where U_d and U_{d+1} are computed using (3). In this regard, V_d is approximately distributed as a Chi-square variate with $(D - d)$ degrees of freedom.

It is important to note that in either test, both *backward* and *forward stepwise* methods can be used. However, in the absence of prior knowledge, Hayashi et al. [2007] recommend using the forward stepwise method as the standard approach for implementing these tests. This approach begins with a one-component model, estimating it and subsequently testing the null hypothesis H_0 with $d = 1$ component. If H_0 is rejected, the process advances by incrementing d by 1, leading to the estimation of a two-component model and a corresponding test for H_0 with $d = 2$ components. Should the rejection of H_0 persist, the process continues with $d = 3$ components, and so on. At each step in this sequence, either or both versions of the LRT can be employed. This iterative process of estimation and testing persists until the null hypothesis H_0 cannot be rejected, at which point the current value of d is taken as the estimated number of components.

3 Numerical Studies

This section aims to strengthen the credibility of our proposal by presenting its reliability across a wide range of relevant scenarios. To accomplish this, we utilize essential numerical studies, including “simulation studies” and “real data”, to assess various properties, including bias. Given the scope of this paper, our simulation study primarily focuses on assessing the performance of TPPCA and PPCA, while performing sensitivity analyses through methods like Cross-Validation (CV), Kaiser-Guttman (KG), and the LRT for estimating the number of components. In contrast, the real-world applications are aimed at evaluating the performance of our proposed method

relative to other PCA-specific extensions for torus data. The insights derived from these numerical analyzes enable researchers to make well-informed decisions when selecting the most appropriate methods to address their specific research questions within their datasets.

3.1 Monte Carlo experiment

Simulation studies are included for various reasons, such as validating theoretical models, evaluating TPPCA algorithm performance, and conducting sensitivity analysis, particularly by utilizing the CV, KG, and LRT for estimating the optimal number of components.

Our goal was to conduct simulation studies with dimensions typically seen in real-world applications. According to the literature (see Sargsyan et al. [2012], Eltzner et al. [2018], Mardia et al. [2022], Zoubouoglou et al. [2022]), RNA datasets are the most relevant, with dimensions up to seven in a hyper-torus. Beyond RNA datasets, we are not aware of any angular real data with dimensions greater than seven. Additionally, due to the high computational cost (See Figures SM-7–SM-8 in Supplementary Material) and limited resources when the dimension exceeds five, we restricted our simulation studies to dimensions of five.

Simulation Design

We evaluate the performance of TPPCA in comparison to PPCA through an extensive Monte Carlo experiment. Our simulation design covers several scenarios, including sample sizes of $N = (50, 100, 500)$, upper dimensions $D = 5$, and lower dimensions $d = (2, 3)$. For simplicity, we set $\boldsymbol{\mu} = 0$ and use an orthonormal matrix \mathbf{W} (generated using the *orth* command in the \mathbb{R} package `pracma`) to relate the variables \mathbf{X} and \mathbf{Z} . Using equations (1) and (2), we generate \mathbf{X} across a range of noise levels, denoted by $\sigma^2 = (\pi/8, \pi/4, \pi/2, \pi, 3\pi/2, 2\pi)$. For each of these scenarios, we conduct a total of 1000 Monte Carlo replications.

The simulation study consists of two parts: In the first part, d is constant at its *true value*. In the second part, we estimate the number of components using various methods such as CV, KG, and LRT.

To assess the performance, we employ several statistical criteria, including

(i) Mean Square Error of the reconstructed \mathbf{X} (denoted as \mathbf{X}^{recons}), i.e.,

$$\text{MSE}(\mathbf{X}^{recons}) = \frac{1}{N} \sum_{i=1}^N (\mathbf{X}_i^{recons} - \mathbf{X}_i^{orig})^2,$$

(ii) Mean Absolute Error of \mathbf{X}^{recons} , i.e.,

$$\text{MAE}(\mathbf{X}^{recons}) = \frac{1}{N} \sum_{i=1}^N |\mathbf{X}_i^{recons} - \mathbf{X}_i^{orig}|,$$

(iii) Mean Square Error of the reconstructed latent variable \mathbf{Z} (noted as \mathbf{Z}^{recons}) as

$$\text{MSE}(\mathbf{Z}^{recons}) = \frac{1}{N} \sum_{i=1}^N (\mathbf{Z}_i^{recons} - \mathbf{Z}_i^{orig})^2,$$

(iv) Mean Absolute Error of \mathbf{Z}^{recons} as

$$\text{MAE}(\mathbf{Z}^{recons}) = \frac{1}{N} \sum_{i=1}^N |\mathbf{Z}_i^{recons} - \mathbf{Z}_i^{orig}|.$$

It is important to note that the term ‘‘orig’’ in \mathbf{X}^{orig} (or \mathbf{Z}^{orig}) denotes the original dataset (or latent variable) used in the simulation study, while ‘‘recons’’ in \mathbf{X}^{recons} (or \mathbf{Z}^{recons}) refers to the reconstructed data (or latent variable) obtained through the TPPCA algorithm, as applied using (1).

Simulation Results

We present a summary of the results in Tables 1–2. Notably, TPPCA consistently outperforms PPCA. As the standard deviation increases, the Mean Square Error (MSE) of \mathbf{X}^{recons} in TPPCA also exhibits an upward trend. Furthermore, the sample size plays a crucial role in enhancing the accuracy of this method. In essence, by accounting for the periodic nature of angles and extending PPCA to TPPCA, significant improvements in the results are achieved. Additionally, as the lower dimension (d) increases, both methods exhibit an increase in these two criteria (i.e., MSE and MAE).

In practical applications, the selection of the lower dimension is challenging. To address this, we conducted a secondary simulation study where we employed CV, KG, and LRT to estimate the number of components (here

Table 1: Performance of the TPPCA and PPCA on the reconstruction of X measured by the MSE and MAE measures using true value of d and $D = 5$.

Lower dim.	Methods	σ^2	MSE(\mathbf{X}^{recons})			MAE(\mathbf{X}^{recons})		
			$n = 50$	$n = 100$	$n = 500$	$n = 50$	$n = 100$	$n = 500$
$d = 2$	TPPCA	$\frac{\pi}{8}$	1.589	1.654	0.879	0.657	0.637	0.460
		$\frac{\pi}{4}$	2.385	2.152	1.500	0.930	0.845	0.671
		$\frac{\pi}{2}$	3.285	3.068	3.068	1.247	1.190	1.145
		π	4.230	4.305	4.159	1.581	1.582	1.529
		$\frac{3\pi}{2}$	4.498	4.634	4.606	1.663	1.684	1.676
		2π	4.950	4.960	4.901	1.747	1.756	1.752
	PPCA	$\frac{\pi}{8}$	16.430	16.324	16.519	3.294	3.289	3.297
		$\frac{\pi}{4}$	15.688	15.465	15.575	3.290	3.253	3.269
		$\frac{\pi}{2}$	14.906	14.395	14.475	3.262	3.224	3.234
		π	14.289	13.915	13.808	3.264	3.240	3.224
		$\frac{3\pi}{2}$	13.917	13.842	13.487	3.250	3.245	3.216
		2π	13.755	13.620	13.156	3.243	3.236	3.211
$d = 3$	TPPCA	$\frac{\pi}{8}$	3.738	2.868	2.397	1.152	0.953	0.788
		$\frac{\pi}{4}$	4.309	4.060	3.092	1.400	1.289	1.039
		$\frac{\pi}{2}$	5.392	5.120	4.512	1.708	1.625	1.448
		π	5.884	6.073	5.919	1.890	1.910	1.865
		$\frac{3\pi}{2}$	6.117	6.415	6.326	1.950	1.990	1.975
		2π	6.376	6.338	6.927	1.997	1.996	2.081
	PPCA	$\frac{\pi}{8}$	18.018	17.852	17.988	3.368	3.344	3.365
		$\frac{\pi}{4}$	17.257	17.459	17.260	3.345	3.368	3.339
		$\frac{\pi}{2}$	16.519	16.448	16.262	3.340	3.341	3.314
		π	16.005	15.562	15.406	3.361	3.317	3.306
		$\frac{3\pi}{2}$	15.370	15.405	15.184	3.328	3.325	3.318
		2π	15.413	15.232	15.037	3.335	3.329	3.310

Table 2: Performance of the TPPCA and PPCA on the reconstruction of Z measured by the MSE and MAE measures using true value of d and $D = 5$.

Lower dim.	Methods	σ^2	MSE(\mathbf{Z}^{recons})			MAE(\mathbf{Z}^{recons})		
			$n = 50$	$n = 100$	$n = 500$	$n = 50$	$n = 100$	$n = 500$
$d = 2$	TPPCA	$\frac{\pi}{8}$	1.943	2.049	1.946	0.991	1.010	0.927
		$\frac{\pi}{4}$	2.460	2.355	1.952	1.197	1.134	0.980
		$\frac{\pi}{2}$	2.664	2.658	2.533	1.285	1.275	1.224
		π	2.560	2.592	2.538	1.290	1.294	1.269
		$\frac{3\pi}{2}$	2.559	2.467	2.398	1.290	1.267	1.243
		2π	2.620	2.410	2.427	1.307	1.253	1.252
	PPCA	$\frac{\pi}{8}$	9.327	9.222	9.388	2.574	2.560	2.570
		$\frac{\pi}{4}$	7.849	7.936	7.722	2.336	2.358	2.329
		$\frac{\pi}{2}$	6.753	6.659	6.425	2.159	2.136	2.108
		π	5.956	5.573	5.202	2.001	1.935	1.872
		$\frac{3\pi}{2}$	5.539	5.218	4.863	1.928	1.865	1.798
		2π	5.395	5.073	4.687	1.901	1.838	1.758
$d = 3$	TPPCA	$\frac{\pi}{8}$	2.343	2.354	2.118	1.168	1.146	1.031
		$\frac{\pi}{4}$	2.642	2.438	2.553	1.285	1.200	1.185
		$\frac{\pi}{2}$	2.579	2.721	2.696	1.280	1.308	1.278
		π	2.483	2.520	2.491	1.264	1.276	1.259
		$\frac{3\pi}{2}$	2.509	2.456	2.499	1.275	1.256	1.267
		2π	2.522	2.439	2.419	1.279	1.257	1.250
	PPCA	$\frac{\pi}{8}$	6.228	6.208	5.731	2.059	2.063	1.970
		$\frac{\pi}{4}$	5.956	5.641	5.559	2.006	1.953	1.944
		$\frac{\pi}{2}$	5.475	5.350	5.161	1.922	1.898	1.870
		π	5.190	5.008	4.792	1.857	1.827	1.787
		$\frac{3\pi}{2}$	5.021	4.877	4.637	1.829	1.796	1.748
		2π	4.949	4.754	4.553	1.817	1.776	1.731

d), as elaborated in Section 2. The performance of TPPCA based on these three different procedures is detailed in Table 3. Our analysis shows minor discrepancies in the performance measures across the three methods, with a slight overall preference for LRT. Detailed results are provided in Section SM-6 of the Supplementary Material. These findings indicate that LRT is the most effective method among those considered for estimating the lower dimension.

3.2 Real Application

To conduct a thorough comparative analysis between our proposed method and various existing approaches in the literature, we selected three distinct datasets: *Sunspots*, as studied by Zoubouloglou et al. [2022]; *small RNA*, and *large RNA (or bigRNA)*, both of which have been previously analyzed by researchers including Eltzner et al. [2018], Nodehi et al. [2021], and Zoubouloglou et al. [2022]. Notably, for the first two real datasets (*Sunspots*, *small RNA*), we conducted a performance comparison of TPPCA against existing methods. However, in the case of *bigRNA*, our aim is to validate simulation results in real-world scenarios. Each of these datasets exhibits unique characteristics and complexities, making them particularly well-suited for the thorough evaluation of our proposed approach in contrast to the methodologies investigated in the studies conducted by the aforementioned researchers.

3.2.1 Sunspots

Sunspots are cooler areas on the Sun’s surface and are closely linked to concentrated magnetic fields on the Sun. These magnetic fields that give rise to sunspots follow a nearly regular 11-year pattern known as the solar cycle. In a study by García-Portugués et al. [2020], they provided a well-organized collection of data on the central points of sunspot groups. Our study specifically examines the most recent solar cycle with comprehensive curated data, which is the 23rd solar cycle. This dataset spans from August 1996 to November 2001 and contains 5373 records. The comprehensive description of sunspots can be found in the paper published by Zoubouloglou et al. [2022]. We investigate the dependence structure of sunspot birth longitudes, denoted by $\theta \in [-\pi, \pi]$. Since the Earth’s rotation around the Sun affects sunspot visibility, we expect a deviation from a linear dependence structure in the series of sunspot longitudes if there are significantly preferred longitudes. To ex-

Table 3: Performance of the TPPCA on the reconstruction of \mathbf{X} measured by the MSE and MAE measures using an estimated value of d by several methods, $D = 5$, true value of d .

Lower dim.	Method	σ^2	MSE(\mathbf{X}^{recons})			MAE(\mathbf{X}^{recons})		
			$n = 50$	$n = 100$	$n = 500$	$n = 50$	$n = 100$	$n = 500$
$d = 2$	CV	$\frac{\pi}{8}$	1.76	1.68	1.09	0.73	0.69	0.53
		$\frac{\pi}{4}$	2.56	2.29	1.67	0.98	0.89	0.71
		$\frac{\pi}{2}$	3.48	3.26	2.58	1.31	1.23	1.03
		π	3.88	3.87	3.92	1.50	1.49	1.46
		$\frac{3\pi}{2}$	4.54	4.25	4.32	1.65	1.60	1.61
		2π	4.56	4.51	4.68	1.67	1.67	1.70
	KG	$\frac{\pi}{8}$	2.18	1.84	1.10	0.80	0.71	0.51
		$\frac{\pi}{4}$	2.74	2.16	1.48	1.00	0.84	0.68
		$\frac{\pi}{2}$	3.39	3.16	2.74	1.29	1.22	1.06
		π	4.48	4.30	4.12	1.61	1.57	1.53
		$\frac{3\pi}{2}$	4.62	4.81	4.72	1.69	1.72	1.70
		2π	4.82	4.73	5.09	1.74	1.72	1.79
	LRT	$\frac{\pi}{8}$	1.75	1.27	1.09	0.72	0.57	0.50
		$\frac{\pi}{4}$	2.72	2.41	1.82	1.02	0.92	0.75
		$\frac{\pi}{2}$	3.44	3.41	3.10	1.32	1.29	1.20
		π	4.56	4.56	4.79	1.66	1.66	1.67
		$\frac{3\pi}{2}$	5.12	5.24	5.41	1.79	1.81	1.84
		2π	5.48	5.38	5.74	1.86	1.86	1.92
$d = 3$	CV	$\frac{\pi}{8}$	4.02	3.18	2.70	1.29	1.09	0.93
		$\frac{\pi}{4}$	4.14	3.96	3.31	1.38	1.30	1.12
		$\frac{\pi}{2}$	4.67	4.64	4.07	1.57	1.54	1.38
		π	5.23	4.92	5.18	1.75	1.69	1.72
		$\frac{3\pi}{2}$	5.45	5.52	5.56	1.83	1.83	1.83
		2π	5.57	5.65	5.88	1.85	1.85	1.90
	KG	$\frac{\pi}{8}$	3.85	3.19	2.82	1.21	1.06	0.94
		$\frac{\pi}{4}$	4.52	3.73	3.27	1.46	1.25	1.10
		$\frac{\pi}{2}$	4.74	4.82	4.13	1.59	1.56	1.38
		π	5.32	5.46	5.33	1.77	1.79	1.75
		$\frac{3\pi}{2}$	5.77	5.91	5.78	1.88	1.91	1.88
		2π	5.75	6.02	6.37	1.88	1.93	1.99
	LRT	$\frac{\pi}{8}$	3.40	3.19	2.35	1.12	1.01	0.78
		$\frac{\pi}{4}$	4.41	3.73	3.39	1.38	1.23	1.11
		$\frac{\pi}{2}$	5.02	5.07	4.63	1.63	1.61	1.49
		π	5.75	6.03	6.33	1.86	1.90	1.92
		$\frac{3\pi}{2}$	6.12	6.19	6.67	1.96	1.97	2.04
		2π	6.25	6.58	7.02	1.98	2.04	2.11

plote this serial structure, we consider the series of longitudes along with its lagged versions of order one and two:

$$\Theta_i = (\theta_i, \theta_{i+1}, \theta_{i+2})^\top \in \mathbb{T}^3, \quad \theta_i \in [-\pi, \pi] \text{ for } i = 1, \dots, 5373.$$

Since the overall dimension of the Sunspots dataset is three, we have three principal component (PC) scores in this dataset. Using a randomly selected sample of 1000 sunspots on the torus, we computed the first PC score based on various methods and determined the proportion of variability explained by each of the three components. This enabled us to provide a detailed comparison between TPPCA and nine other dimension reduction techniques.

One limitation of T-PCA [Eltzner et al., 2018] is that it introduces distortion when it transforms the hyper-torus (\mathbb{T}^3) into the hypersphere (\mathbb{S}^3). This distortion leads to an artificial clustering pattern in the first scores, as illustrated in Figures 1(b) and 1(c), even though the marginal values of Θ_i are uniformly distributed. In contrast, our proposed method (Figure 1(d)) and ST-PCA (Figure 1(a)) demonstrate a uniform distribution. As recommended by Zoubouloglou et al. [2022], we conducted a formal comparison of the distributions of the first scores from TPPCA, T-PCA (SI), T-PCA (SO), and ST-PCA. This was done through three omnibus circular uniformity tests, using their asymptotic distributions as implemented in the `sphunif` package in \mathbb{R} [García-Portugués and Verdebout, 2021]. The results, summarized in Table 4, show that the uniformity hypothesis cannot be rejected for the marginal distribution of the original longitudes (Θ_i), as well as the corresponding scores for TPPCA and ST-PCA. However, the hypothesis is rejected for the scores obtained from the two possible orderings of T-PCA.

We also conducted a comprehensive comparison between TPPCA and nine other dimension reduction techniques as suggested by Zoubouloglou et al. [2022]. For each method, we calculated the percentage of variability explained by their three components. Our findings are summarized in Table 5. It is important to note that existing software for GeoPCA primarily employs PGA and provides information on the variance explained by the first two components rather than the total variance explained. Consequently, we omitted GeoPCA from Table 5. Notably, TPPCA and ST-PCA stand out for explaining the highest proportion of variance through their first principal components compared to their competitors.

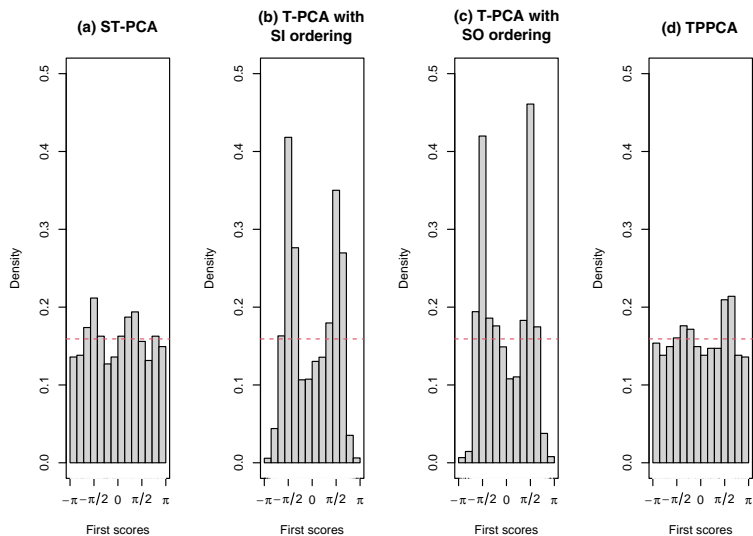


Figure 1: Histograms representing the first score of different methods are shown as follows: (a) ST-PCA; (b) T-PCA with SI ordering; (c) T-PCA with SO ordering; (d) TPPCA. Both versions of T-PCA reveal the presence of unexpected clusters, despite the marginal distributions of the data not significantly deviating from uniformity. In contrast, ST-PCA and TPPCA do not display these spurious clusters.

Table 4: p-values for various circular uniformity tests.

Test	Longitudes	ST-PCA	TPPCA	T-PCA (SO)	T-PCA (SI)
Giné's Fn	0.32	0.08	0.30	<0.001	<0.001
Watson	0.35	0.18	0.40	<0.001	<0.001
Projected Anderson-Darling	0.75	0.13	0.40	<0.001	<0.001

Note: From left to right column: name of the test; p-values for testing uniformity on the original longitudes; p-values for testing uniformity on the first scores of the corresponding method. The original longitudes, ST-PCA and TPPCA's first scores are not significantly nonuniform, while uniformity is rejected in T-PCA's first scores.

Table 5: Percentage of variance explained by components of dimension reduction methods on the torus, sorted decreasingly according to the percentage of variance explained by their first components.

Methods	Component 1	Component 2	Component 3	Total percentage explained
ST-PCA	90.51	3.07	6.41	100
TPPCA	90.28	5.19	4.53	100
T-PCA (SO)	89.32	6.43	4.25	100
T-PCA (SI)	88.27	6.97	4.76	100
Complex dPCA	72.51	14.59	12.90	100
PCA	55.43	24.48	20.09	100
aPCA	43.27	31.28	25.45	100
dPCA+	42.69	30.53	26.78	100
dPCA	38.48	34.06	7.67	80.21
PPCA	37.44	37.44	25.12	100

Note: TPPCA and ST-PCA explain the most percentage of variance in their first component. The dPCA gives a six-dimensional embedding and, as a result, the sum of the variance explained by the first three dimensions does not add up to 100%.

3.2.2 Small RNA data sets

The RNA datasets have been frequently employed in the literature [Sargsyan et al., 2012, Eltzner et al., 2018, Mardia et al., 2022, Zoubouloglou et al., 2022] to assess and validate PCA methods designed for toroidal data. In RNA data, each nucleic base corresponds to a backbone segment described by 6 dihedral angles and one angle for the base, giving a total of 7 angles. The small RNA data set contains 181 observations, which form three clusters in the $\eta - \theta$ plot as shown in Figure 2. The $\eta - \theta$ plot is a graphical tool used to capture the conformational landscape of RNA molecules by plotting two pseudo-torsion angles, η and θ . Each point on the plot represents a specific nucleotide position, with clusters of points indicating regions of similar conformations. This plot is particularly useful for identifying structural patterns and differences within the RNA molecule [Duarte and Pyle, 1998, Sargsyan et al., 2012].

In this section, our primary focus centers on examining four distinct methods that exhibit the highest proportion of variance through their first component in *Sunspots*. These methods of interest include (a) TPPCA, (b) ST-PCA, (c) T-PCA with SI ordering, and (d) T-PCA with SO ordering. These methods were selected based on their ability to capture the most variance within their initial components. A thorough analysis was performed, considering all four algorithms, and the findings are presented in Figure 3.

Remarkably, following the identification of three clusters in the $\eta - \theta$ plot, it is worth highlighting that both TPPCA and ST-PCA consistently group the data into three distinctive clusters when evaluating the first two principal components. To quantify the overlap between the clusters identified in the $\eta - \theta$ plot and those found by the first two principal components, we calculated the Adjusted Rand Index (ARI) for each method [Hubert and Arabie, 1985]. The ARI values are as follows: ST-PCA (ARI=0.71), TPPCA (ARI=0.64), T-PCA (SI) (ARI=0.22), and T-PCA (SO) (ARI=0.53). These results indicate that ST-PCA and TPPCA show good agreement with the clusters from the $\eta - \theta$ plot, suggesting a high degree of consistency. In contrast, T-PCA (SI) and T-PCA (SO) show lower overlap, with T-PCA (SI) demonstrating the least agreement. The high ARI values for TPPCA and ST-PCA underscore their robustness in accurately capturing the underlying cluster structure in RNA data.

To assess the quality of our clustering results, follow the recommendations provided by Brock et al. [2008], Koutroumbas and Theodoridis [2008] and Charrad et al. [2014]. These authors suggest employing clustering validation statistics, including direct comparisons and statistical testing methods. The following three criteria are used for this purpose:

1. **Elbow plot** [Kaufman and Rousseeuw, 2009] seeks to find clusters in a manner that minimizes the cumulative sum of squares within each cluster, often referred to as the within-cluster sum of squares (WSS). The point at which an “elbow” is observed in the plot is conventionally considered an indicator of the most suitable number of clusters. However, there are some limitations. The exact elbow point can sometimes be ambiguous or subjective. In some datasets, especially those with clusters of varying density or size, the elbow method might not yield a clear point of inflection. This is pretty common in real-world datasets.
2. **Average silhouette** [Kaufman and Rousseeuw, 2009] computes the mean silhouette value for data points across various cluster numbers, denoted as k . The optimal number of clusters, represented by k , is the one that maximizes the average silhouette across a range of potential cluster values.
3. **The gap statistic** [Tibshirani et al., 2001] provides a robust method of determining the optimal number of clusters. It involves comparing the total within-cluster variation for different values of $k > 1$ with their

expected values under a null reference distribution, which is generated by randomly sampling data points from a uniform distribution over the range of the observed data. By measuring how much better the observed clustering is compared to random clustering, the gap statistic identifies the optimal number of clusters as the value that maximizes the gap statistic. This method is considered robust for determining the number of clusters, as it distinguishes meaningful clustering structures from those expected by chance.

Figure 4 provides a visualization of the optimal number of clusters for the RNA dataset using the first two principal components of TPPCA, ST-PCA, T-PCA (SI), and T-PCA (SO). We used three criteria to determine the optimal number of clusters: the elbow method, the average silhouette, and the gap statistic.

The elbow method, presented in the first column of Figure 4, involves identifying the point where the within-cluster sum of squares starts to level off, although this method is somewhat subjective. The second column of Figure 4 shows the results for the average silhouette method, which identifies the optimal number of clusters by maximizing the average silhouette score across various potential cluster counts, with the optimal value indicated by the vertical line. Notably, TPPCA and ST-PCA were the only methods that suggested a number of clusters closely matching the true value. Finally, the third column of Figure 4 illustrates the results of the gap statistic method, which identifies the number of clusters that maximize the gap statistic value, as indicated by the vertical line. According to Tibshirani et al. [2001], the gap statistic is considered the most robust criterion for determining the optimal number of clusters.

3.2.3 Large RNA data set (*bigRNA*)

In our previous practical applications, we compared the performance of TP-PCA against other established methods. This section now aims to validate the simulation results in real-world scenarios. Our objective is to apply TP-PCA and compare the performance of the LRT, KG, and CV criteria in terms of explaining a higher proportion of variability. To achieve this, we used a large RNA dataset, also known as *bigRNA*, which has been previously analyzed in the studies by Eltzner et al. [2018] and Nodehi et al. [2021]. The original data set initially consisted of 8301 observations in seven dimensions. For the *bigRNA* dataset, a deviation of 50° in torus distance from the

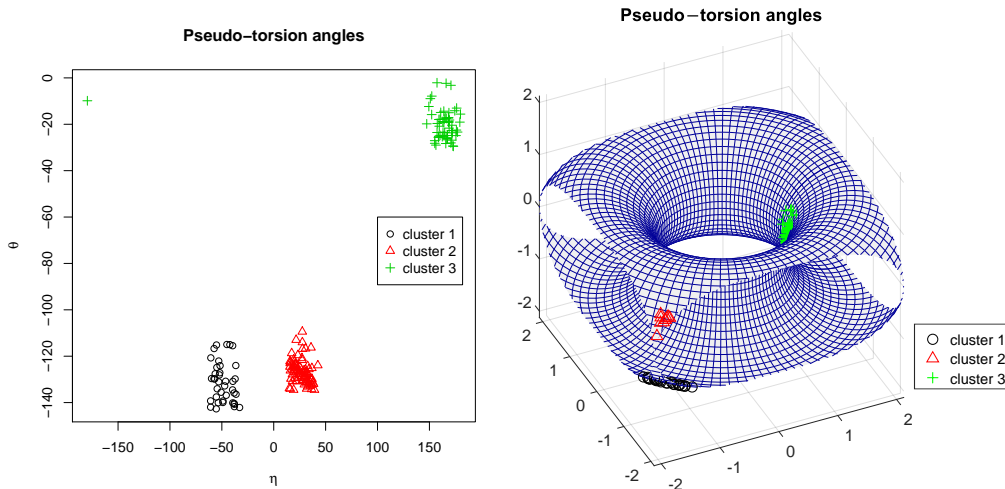


Figure 2: RNA data set. Their three preselected clusters in the $\eta - \theta$ plot in $2D$ and on the torus.

nearest neighbor, based on visual inspection, was used to identify outliers. Observations deviating by more than 50° in angular distance were labeled as outliers and excluded from the analysis. The dataset was divided into 23 clusters using single linkage hierarchical clustering with a branch-cutting heuristic. Consequently, the final dataset comprises 7390 observations distributed across the 23 clusters.

We applied the proposed TPPCA algorithm to this data set and the results to select the number of components across the 23 clusters are presented in Table SM-1 (in the Supplementary Material). Consistent with our simulation studies, the LRT criterion outperformed the others in this real-world scenario. Table SM-1 highlights the effectiveness of LRT, showing a higher cumulative percentage of explained variance compared to the KG and CV criteria. These findings further support the robustness and practical use of the LRT, as demonstrated in both our simulations and real-world applications.

4 Conclusions

We have developed a novel algorithm for extracting information from torus data, thoroughly evaluating its performance through extensive simulation

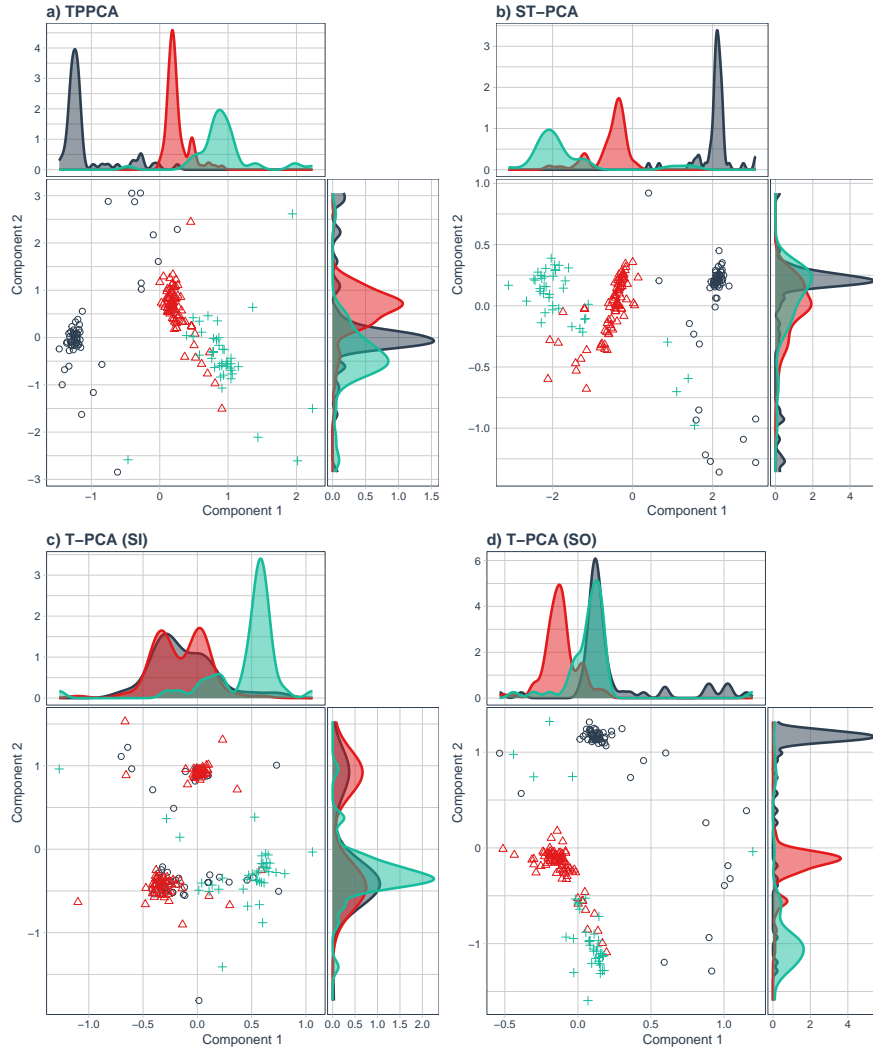


Figure 3: Visualizations of the two-dimensional representation of the first two components are provided for a) TPPCA, b) ST-PCA, c) T-PCA (SI), and d) T-PCA (SO) applied to the RNA dataset. Kernel density estimation is utilized to examine modality, with the analysis focusing on the distribution of the first and second scores presented on the horizontal and vertical axes, respectively.

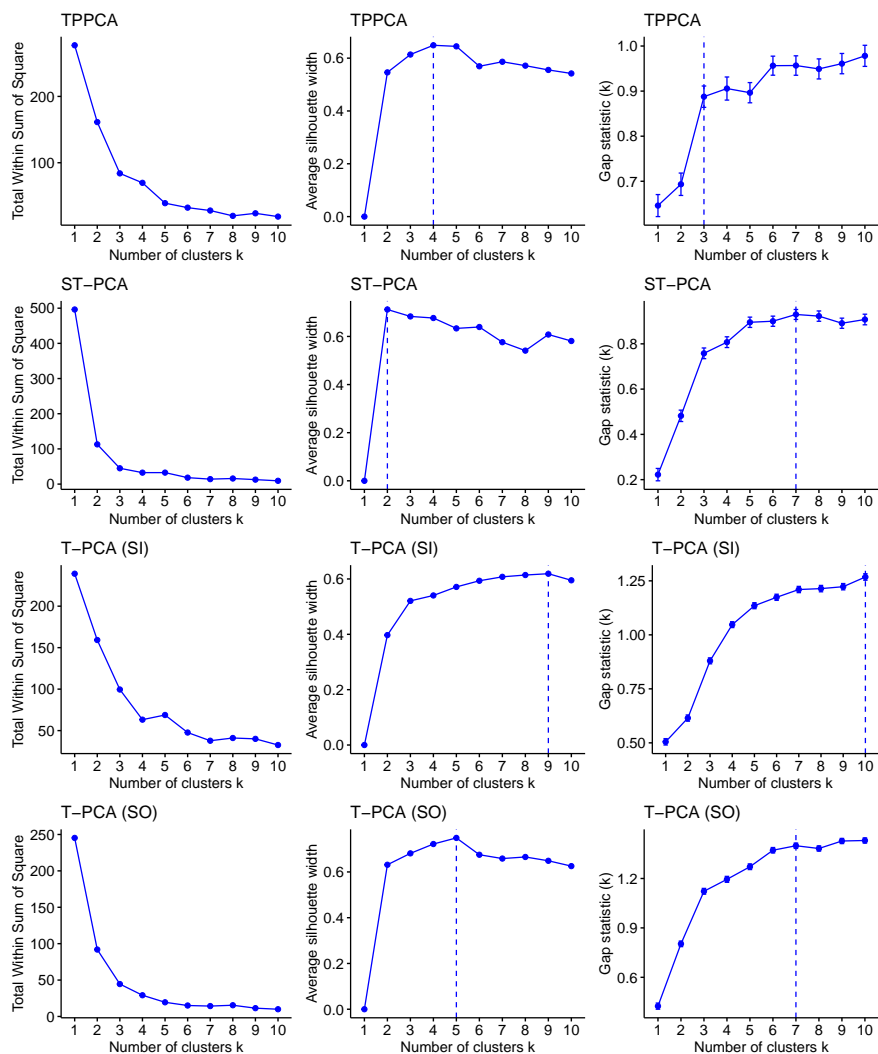


Figure 4: Visualization of the optimal number of clusters based on the first two components in TPPCA, ST-PCA, T-PCA with SI ordering (denoted as T-PCA (SI)), and T-PCA with SO ordering (denoted as T-PCA (SO)) for the RNA dataset.

studies and practical real-world applications.

When applied to Euclidean data, both probabilistic and classical PCA are valid and yield the same results. However there are a few distinct advantages of employing probabilistic PCA, such as its potential to work with probabilistic models, perform statistical testing, and apply Bayesian approaches. Matrix decomposition and the EM algorithm are the two parameter estimation methods that Tipping and Bishop [1997] suggested. In TPPCA, the proposed iterative algorithm, which integrates the CEM algorithm in the first step, refines the estimates for $\boldsymbol{\mu}$, \mathcal{K} , \mathbf{W} , and σ^2 until convergence. Unlike the approach in Nodehi et al. [2021], which focused solely on estimating $\boldsymbol{\mu}$ and \mathcal{K} with a general covariance structure, the present work extends this by also estimating the loading matrix \mathbf{W} associated with the principal components of the wrapped normal model and σ^2 . This extension enables a more comprehensive analysis of toroidal data using TPPCA.

The implications for the toroidal variables are significant. Specifically, while the eigenvalue-based solution still holds for unwrapped variables in the Euclidean setting, for toroidal data, the estimation process must account for the periodicity and the manifold structure. This difference necessitates a modified approach in TPPCA, where the wrapping of variables is taken into consideration during inference. As a result, the interpretation of the loading matrix \mathbf{W} in the context of toroidal variables differs from that in the classical Euclidean setting.

To determine the optimal number of components, we introduced a novel approach based on LRT. This statistical framework allows us to make informed decisions about the most suitable number of components to retain. To validate the effectiveness of TPPCA, we used it in real-world data analysis. Specifically, we applied TPPCA to three distinct datasets: one dealing with the occurrence of sunspots and two RNA datasets. The results from these applications indicated that both TPPCA and ST-PCA outperformed existing methods across various evaluation criteria. This demonstrates the advantages and potential of our approach for real-world datasets, emphasizing its capability to enhance data analysis tasks.

Like any framework, our proposal is not without limitations. Techniques like PCA, while beneficial, do involve a trade-off, namely, information loss. Striking a balance between feature extraction and preserving critical information represents a crucial compromise inherent to utilizing PCA on a torus. Moreover, it is essential to know that the EM algorithm can be sensitive to local extrema. To mitigate this sensitivity, it is recommended to run the

algorithm with a range of initial values, improving its robustness and reliability. Overall, despite its limitations, our proposal provides a valuable tool for analyzing toroidal data and is applicable across a wide range of fields.

Acknowledgements

The authors extend their gratitude to Eltzner et al. [2018] and Zoubouoglou et al. [2022] for their contribution in preparing the real dataset.

Data Availability

The datasets employed in this study are publicly accessible through R and have been sourced from previously published works [Eltzner et al., 2018, Zoubouoglou et al., 2022]. Specifically, the Sunspots dataset is available within the `rotasym` package on R, while the Small RNA dataset can be found in the supplementary material of [Zoubouoglou et al., 2022] (please refer to here). The large RNA (*bigRNA*) dataset is accessible via the following link: here [Eltzner et al., 2018]. Additionally, the R codes used in this study are available upon request from the first author.

Supplementary Material

The Supplementary Material provides extensive additional content, including a review of the Probabilistic Principal Component Analysis (PPCA) in Section SM-1 and a thorough examination of manifold structures in Section SM-2. Section SM-3 provides a detailed discussion of PCA techniques specifically adapted for toroidal data. Furthermore, Section SM-4 expands on the methodology behind Torus Probabilistic PCA (TPPCA). The theoretical foundations for selecting the optimal number of components using Cross-Validation (CV) are explored in Section SM-5. Section SM-6 presents comprehensive results from simulation studies, while Section SM-7 highlights a real-world application involving an RNA dataset with 23 groups across 7 variables and varying sample sizes. This supplementary material is a valuable resource for a deeper understanding of the concepts and methodologies discussed in the main text.

SM-1 A review on Probabilistic Principal Component Analysis (PPCA)

There are two formulations of PCA found in the literature. The first defines PCA as an orthogonal projection of the data onto a lower-dimensional linear space, termed the principal subspace, with the objective of maximizing the variance of the projected data, a concept introduced by Hotelling [1933]. The second formulation characterizes PCA as a linear projection that minimizes the average projection cost. This cost is determined by the mean squared distance between the data points and their respective projections. Furthermore, PCA is a linear transformation of variables to create new uncorrelated combined variables. The discussed definition of PCA is rooted in linear projection of the data onto a subspace with lower dimensionality than the original data space, a concept initially articulated by Pearson [1901].

The Probabilistic Principal Component Analysis (PPCA) is an extension of PCA that provides several advantages compared to classical PCA. Incorporating a probabilistic model with a measure of likelihood enables the capacity to conduct comparisons with other probabilistic methodologies and enables the application of statistical testing and Bayesian approaches. In addition, the use of a probabilistic model and Expectation-Maximization (EM) algorithm improves the ability of the PPCA to effectively address the is-

sue of missing values in datasets. Further, the PPCA can also be used to model class-conditional densities, and hence can be applied to classification problems.

A latent variable model seeks to relate a D -dimensional observation vector \mathbf{X} to a corresponding d -dimensional vector of latent (or unobserved) variables \mathbf{Z} ($d < D$), using the model

$$\mathbf{X} = \boldsymbol{\mu} + \mathbf{W}\mathbf{Z} + \boldsymbol{\epsilon}$$

where \mathbf{W} is a $(D \times d)$ matrix that relates the two sets of variables, $\mathbf{X} = (X_1, \dots, X_D)^\top$, $\mathbf{Z} = (Z_1, \dots, Z_d)^\top$, while the parameter vector $\boldsymbol{\mu}$ allows the model to have a non-zero mean. The vector $\mathbf{Z} \sim N_d(\mathbf{0}, \mathbf{I}_d)$ is an d -dimensional Gaussian latent variable, and $\boldsymbol{\epsilon} \sim N_D(\mathbf{0}, \sigma^2 \mathbf{I}_D)$ is a D -dimensional zero-mean Gaussian-distributed noise variable with covariance $\sigma^2 \mathbf{I}_D$. We assume $\text{Cov}(\mathbf{Z}, \boldsymbol{\epsilon}) = \mathbf{0}$. Then, we obtain,

$$\mathbb{E}(\mathbf{X}) = \mathbb{E}(\boldsymbol{\mu} + \mathbf{W}\mathbf{Z} + \boldsymbol{\epsilon}) = \boldsymbol{\mu}$$

and

$$\text{Cov}(\mathbf{X}) = \mathbb{E}[(\boldsymbol{\mu} + \mathbf{W}\mathbf{Z} + \boldsymbol{\epsilon})(\boldsymbol{\mu} + \mathbf{W}\mathbf{Z} + \boldsymbol{\epsilon})^\top] = \mathbf{W}\mathbf{W}^\top + \sigma^2 \mathbf{I}_D = \mathbf{C}.$$

Tipping and Bishop [1997] introduced two methods to estimate the parameters: matrix decomposition and the Expectation-Maximization (EM) algorithm. Notably, the EM algorithm offers a notable advantage, particularly in large-scale applications, due to its computational efficiency, as highlighted by Roweis [1998]. Furthermore, the EM algorithm considers an interesting limit where $\sigma^2 \rightarrow 0$ corresponds to the classical PCA, as noted by Roweis [1998].

SM–2 A review on manifold

Manifolds are a fundamental concept in mathematics and geometry, playing a crucial role in various scientific disciplines, including differential geometry, topology, and data analysis. In this section, we briefly review some relevant concepts of manifolds based on Karcher [1977], Boothby [1986], Fletcher et al. [2004] and Pennec [2006].

Definition 1 *Let \mathcal{X} and \mathcal{Y} be topological spaces. A mapping $f : \mathcal{X} \rightarrow \mathcal{Y}$ is a homeomorphism if it is bijective and both f and f^{-1} are continuous. In this case \mathcal{X} and \mathcal{Y} are said to be homeomorphic.*

Definition 2 A topological space \mathcal{X} is said to be Hausdorff if for any two distinct points $x, y \in \mathcal{X}$, there exist disjoint open sets U and V with $x \in U$ and $y \in V$.

A *manifold* is a topological space that is locally equivalent to Euclidean space. More precisely,

Definition 3 (Manifold) A manifold M is a Hausdorff space with a countable basis such that for each point $p \in M$ there is a neighborhood U of p that is homeomorphic to Euclidean space \mathbb{R}^n for some integer n .

Lines and circles are classic examples of one-dimensional manifolds, while two-dimensional manifolds are commonly referred to as surfaces. Notable instances include the plane, the sphere, and the torus. The concept of a manifold is foundational in geometry and non-Euclidean spaces, as it enables the representation of intricate structures in terms of well-understood topological properties from simpler spaces. Manifolds serve as a fundamental framework, facilitating the understanding and characterizing complex geometric spaces.

According to Karcher [1977], for each manifold $M \subset \mathbb{R}^d$, it is possible to associate a linear subspace of \mathbb{R}^d to each point $x \in M$. This space is called the *tangent space* at x , and is written as $T_x M$.

Definition 4 (Tangent space) The tangent space $T_x M$ is the set of tangent vectors of all curves passing through the point $x \in M$. Intuitively, a linear subspace best approximates the manifold M in a neighborhood of the point x . It is equipped with an inner product

$$g_x : T_x M \times T_x M \longrightarrow \mathbb{R}$$

along with a norm metric $\|\cdot\| : T_x M \rightarrow \mathbb{R}$ defined by $\|\nu\| := \sqrt{g_x(\nu, \nu)}$ for any $\nu \in T_x M$.

A well-known theorem states that for any given Riemannian manifold denoted as M , there exists an isometric embedding into the Euclidean space, given that the dimension of the Euclidean space is chosen to be sufficiently large. This theorem is famously attributed to the work of *John Nash* [Boothby, 1986] and remains a celebrated cornerstone in the field of differential geometry.

Definition 5 (Riemannian manifold) *A Riemannian manifold, denoted as M , is a type of smooth manifold characterized by the presence of a metric, denoted as g_x , which smoothly varies and serves as an inner product on the tangent space T_xM at each point x within the manifold. This family of inner products, collectively referred to as a Riemannian metric, defines the geometric properties of the manifold.*

Distances within a manifold are crucial for establishing measures of centrality and dispersion in directional statistics. The **geodesic**, defined as the shortest curve connecting a pair of points on the manifold, is the fundamental concept in this context.

Definition 6 (Geodesic curve) *Given a couple of points on a Riemannian manifold $(p, q) \in M$ and the set of all curves $\gamma : [a, b] \rightarrow M$ such that $\gamma(a) = p$ and $\gamma(b) = x$. Suppose that a Riemannian manifold M is pathwise connected, in the sense that for any two points p, q there exists a smooth path $\gamma : [a, b] \rightarrow M$ such that $\gamma(a) = p$ and $\gamma(b) = q$, the geodesic curve $\bar{\gamma}$ is the curve with the shortest total length from p to q .*

SM–3 A review on extending of the PCA on torus

Torus-specific PCA techniques have emerged from the need to analyze dihedral angles in proteins or RNA within bioinformatics, as demonstrated in previous research [Mu et al., 2005, Altis et al., 2007, Nodehi et al., 2015, Eltzner et al., 2018, Nodehi et al., 2021, Zoubouloglou et al., 2022, Mardia et al., 2022]. In our real-world application, we explore several modern torus data techniques that facilitate the practical use of these comparative methods. These techniques include:

1. Dihedral angles principal component analysis (dPCA):

Mu et al. [2005] and Altis et al. [2007] introduced dPCA as an extension of PCA designed for dihedral angles in proteins. The fundamental concept underlying dPCA involves applying PCA to dihedral angles after they have been transformed into sinusoidal and cosinusoidal representations. The transformation from the angular space to a linear

metric coordinate space is achieved through the utilization of trigonometric functions. However, the dPCA exhibits several limitations. Notably, it requires twice the number of variables, overlooks the identity $\cos^2 \theta + \sin^2 \theta = 1$, and fails to account for the topological characteristics of angles. These constraints have motivated researchers to explore alternative extensions of dPCA.

2. **Angular PCA (aPCA):**

Riccardi et al. [2009] introduced Angular PCA (aPCA) specifically tailored for toroidal data, centered on their circular means. This approach, as demonstrated by Riccardi et al. [2009], yields free-energy landscapes that exhibit a striking similarity to those produced by dPCA.

3. **Complex dPCA:**

Altis et al. [2007] introduced Complex dPCA as an alternative extension to dPCA for toroidal data. Let $\theta_j \in [0, 2\pi]$ represent an angle. One can transform θ_j into complex numbers using Euler's formula:

$$z_j = e^{i\theta_j} \quad (j = 1, \dots, N).$$

The covariance matrix corresponding to the complex variables z_j is defined as:

$$C_{kj} = \langle (z_k - \langle z_k \rangle)(z_j^* - \langle z_j^* \rangle) \rangle$$

where $k, j = (1, \dots, N)$, z^* denotes the complex conjugate of z , and $\langle \dots \rangle$ represents the average over all sampled conformations. The matrix \mathbf{C} is Hermitian, possessing N real-valued eigenvalues λ_j and N complex eigenvectors ν_j ,

$$\mathbf{C}\nu_j = \lambda_j\nu_j$$

The complex principal components are expressed as:

$$Y_j^{\text{Complex}} = \nu_j^\top \mathbf{z}.$$

In summary, Complex dPCA is an extension of dPCA that transforms dihedral angles into complex numbers using Euler's formula. The covariance matrix is defined using the complex variables, and the resulting complex eigenvectors and eigenvalues can be used to compute the complex principal components.

4. **PCA on torus (dPCA+):**

Dihedral angles principal component analysis plus (dPCA+) is an extension of dPCA for torus data [Sittel et al., 2017]. The method aims to minimize the projection error induced by periodicity by transforming the data such that the maximal gap of the sampling is shifted to the periodic boundary. The covariance matrix and its eigen-decomposition can then be computed in a standard manner. This method preserves the topological feature of the torus by defining the data points' correct neighborhoods. However, the main assumption underlying dPCA+ is that the data show a significant gap in their distribution, which is a limitation in general. Additionally, dPCA+ is relatively comparable to angular PCA (aPCA) [Riccardi et al., 2009] in its practical application.

5. **Torus principal component analysis (T-PCA):**

The T-PCA is an extension of PCA to torus data, as suggested by Eltzner et al. [2018]. This method deforms tori into spheres and then uses PNS [Jung et al., 2012]. However, deforming tori into spheres creates singularities, which the authors circumvent by introducing a data-adaptive pre-clustering technique to avoid singularities. The authors proposed two data-driven orderings of variables, *SI ordering* and *SO ordering*, corresponding to sorting the variables in terms of descending and increasing amount of circular spread, respectively. However, Zoubouloglou et al. [2022] showed that *SI ordering* and *SO ordering* yield significantly different outcomes that may affect subsequent analyses.

6. **Scaled torus principal component analysis (ST-PCA):**

The ST-PCA was recently proposed by Zoubouloglou et al. [2022] as a method for analyzing multivariate toroidal data. ST-PCA seeks a data-driven map from a torus to a sphere with the same size and radius as the torus. The method is based on the idea that spherical embeddings are more appropriate than Euclidean ones when considering transformations from d -torus, \mathbb{T}^d , as proposed by Eltzner et al. [2018]. The analyses are done on spheres, and after finding the best fit of data, it can be inverted back to the torus. To minimize the disparity between pairwise geodesic distances in both spaces, the map is built via multidimensional scaling [Cox and Cox, 1991, 2008].

SM–4 A review on TPPCA

In this section, we provide a more detailed explanation of TPPCA, as referenced in the main paper.

SM–4.1 Step 0: Initial values

In this section, we outline the procedure for selecting suitable initial values for the parameters ($\boldsymbol{\mu}$, \mathbf{W} , and σ^2) and impute the missing values \mathcal{K} in the model. The initial values for the EM algorithm are obtained through a two-step process:

1. Estimation of initial values for \mathcal{K} : In this step, an unstructured variance-covariance matrix $\boldsymbol{\Sigma}$ is assumed, such that $\mathbf{Y} \sim WN_D(\boldsymbol{\mu}, \boldsymbol{\Sigma})$. Initial values $\hat{\mathcal{K}}_0 = (\hat{\mathbf{k}}_1, \dots, \hat{\mathbf{k}}_N)$ are obtained using the Classification Expectation-Maximization (CEM) algorithm proposed by Nodehi et al. [2021].
2. Estimation of initial values for the remaining parameters: a strategy similar to that used by Tipping and Bishop [1999] is employed to maximize the log-likelihood $\ell(\boldsymbol{\mu}, \mathbf{W}, \sigma^2, \hat{\mathcal{K}}_0)$ with respect to the parameters, yielding the initial estimates $(\hat{\boldsymbol{\mu}}_0, \hat{\mathbf{W}}_0, \hat{\sigma}_0^2)$. These estimates are then used to initiate the iterative algorithm (Steps 1 and 2). For more details on PPCA, please refer to SM-1.

SM–4.2 Step 1

The update of $\boldsymbol{\mu}$ and \mathcal{K} can be performed as outlined in [Nodehi et al., 2021], using the CEM algorithm. The CEM algorithm, when applied to $\Gamma(\boldsymbol{\mu}, \hat{\mathbf{W}}, \hat{\sigma}^2, \mathcal{K}|\mathcal{Y})$, is an iterative classification algorithm that performs the estimation of the parameter ($\boldsymbol{\mu}$) and the imputation of missing classification (\mathcal{K}).

- **E step (Expectation)**: The expectation of log-likelihood over the latent variables based on the data samples and initial values as shown in $\Gamma(\boldsymbol{\mu}, \hat{\mathbf{W}}, \hat{\sigma}^2, \mathcal{K}|\mathcal{Y})$.

- **C step (Classification):** Update $\hat{\mathcal{K}}$ by

$$\begin{aligned}\hat{\mathcal{K}} &= \arg \max_{\mathcal{K} \in \mathbb{Z}^D} \sum_{j=1}^N \Gamma(\hat{\boldsymbol{\mu}}, \hat{\mathbf{W}}, \hat{\sigma}^2, \mathcal{K} | \mathcal{Y}) \\ &= \arg \max_{\mathbf{k}_j \in \mathbb{Z}^D, j=1, \dots, N} \sum_{j=1}^N \Gamma(\hat{\boldsymbol{\mu}}, \hat{\mathbf{W}}, \hat{\sigma}^2, \mathbf{k}_j | \mathbf{y}_j),\end{aligned}$$

which is equivalent to maximizing component by component $\Gamma(\hat{\boldsymbol{\mu}}, \hat{\mathbf{W}}, \hat{\sigma}^2, \mathbf{k}_j | \mathbf{y}_j)$, i.e.

$$\hat{\mathbf{k}}_j = \arg \max_{\mathbf{k}_j \in \mathbb{Z}^D} \Gamma(\hat{\boldsymbol{\mu}}, \hat{\mathbf{W}}, \hat{\sigma}^2, \mathbf{k}_j | \mathbf{y}_j), \quad j = 1, \dots, N.$$

- **M step (Maximization):** Using equation (2) in the paper, and considering $\Gamma(\boldsymbol{\mu}, \hat{\mathbf{W}}, \hat{\sigma}^2, \hat{\mathcal{K}} | \mathcal{Y})$ we update $\hat{\boldsymbol{\mu}}$ by evaluating

$$\begin{aligned}\frac{\partial \Gamma(\boldsymbol{\mu}, \hat{\mathbf{W}}, \hat{\sigma}^2, \hat{\mathcal{K}} | \mathcal{Y})}{\partial \boldsymbol{\mu}} &= \\ \sum_{j=1}^N \left[\frac{(\mathbf{y}_j + 2\pi \hat{\mathbf{k}}_j - \boldsymbol{\mu})^\top}{\sigma^2} - \frac{\mathbb{E}(\mathbf{Z}_j^\top | \mathbf{y}_j + 2\pi \hat{\mathbf{k}}_j) \mathbf{W}^\top}{\sigma^2} \right] &= \\ \sigma^{-2} \sum_{j=1}^N (\mathbf{y}_j + 2\pi \hat{\mathbf{k}}_j - \boldsymbol{\mu})^\top - \sum_{j=1}^N (\mathbf{y}_j + 2\pi \hat{\mathbf{k}}_j - \boldsymbol{\mu})^\top \mathbf{W} \mathbf{M}^{-1} \mathbf{W}^\top,\end{aligned}$$

equating it to $\mathbf{0}$ and solving for $\boldsymbol{\mu}$ leads to

$$N \boldsymbol{\mu}^\top (\mathbf{I}_D - \mathbf{W} \mathbf{M}^{-1} \mathbf{W}^\top) = \sum_{j=1}^N (\mathbf{y}_j + 2\pi \hat{\mathbf{k}}_j)^\top (\mathbf{I}_D - \mathbf{W} \mathbf{M}^{-1} \mathbf{W}^\top)$$

that is

$$\hat{\boldsymbol{\mu}} = \frac{\sum_{j=1}^N (\mathbf{y}_j + 2\pi \hat{\mathbf{k}}_j)}{N} = \frac{\sum_{j=1}^N \hat{\mathbf{x}}_j}{N}$$

where $\hat{\mathbf{x}}_j = \mathbf{y}_j + 2\pi \hat{\mathbf{k}}_j$ is an estimate of the unobserved \mathbf{x}_j ($j = 1, \dots, N$).

SM-4.3 Step 2

Considering the derivative of the function $\Gamma(\hat{\boldsymbol{\mu}}, \mathbf{W}, \sigma^2, \hat{\mathcal{K}}|\mathcal{Y})$ with respect to the variables \mathbf{W} and σ^2 , this could be formulated as follows:

$$\frac{\partial \Gamma(\hat{\boldsymbol{\mu}}, \mathbf{W}, \sigma^2, \hat{\mathcal{K}}|\mathcal{Y})}{\partial \mathbf{W}} = \sum_{j=1}^N \left[-\frac{\mathbf{W} \mathbb{E}(\mathbf{Z}_j \mathbf{Z}_j^\top | \hat{\mathbf{x}}_j)}{2\sigma^2} + \sigma^{-2} (\hat{\mathbf{x}}_j - \hat{\boldsymbol{\mu}}) \mathbb{E}(\mathbf{Z}_j^\top | \hat{\mathbf{x}}_j) \right],$$

we obtain

$$\begin{aligned} \hat{\mathbf{W}} &= \left[\sum_{j=1}^N (\hat{\mathbf{x}}_j - \hat{\boldsymbol{\mu}}) \mathbb{E}(\mathbf{Z}_j^\top | \hat{\mathbf{x}}_j) \right] \left[\sum_{j=1}^N \mathbb{E}(\mathbf{Z}_j \mathbf{Z}_j^\top | \hat{\mathbf{x}}_j) \right]^{-1} \\ &= \left[\sum_{j=1}^N (\hat{\mathbf{x}}_j - \hat{\boldsymbol{\mu}}) (\hat{\mathbf{x}}_j - \hat{\boldsymbol{\mu}})^\top \mathbf{W} \mathbf{M}^{-1} \right] \times \\ &\quad \left[N\sigma^2 \mathbf{M}^{-1} + \sum_{j=1}^N \mathbf{M}^{-1} \mathbf{W}^\top (\hat{\mathbf{x}}_j - \hat{\boldsymbol{\mu}}) (\hat{\mathbf{x}}_j - \hat{\boldsymbol{\mu}})^\top \mathbf{W} \mathbf{M}^{-1} \right]^{-1} \\ &= \mathbf{S} \mathbf{W} \mathbf{M}^{-1} \{ \sigma^2 \mathbf{M}^{-1} + (\mathbf{M}^{-1} \mathbf{W}^\top \mathbf{S} \mathbf{W} \mathbf{M}^{-1}) \}^{-1} \\ &= \mathbf{S} \mathbf{W} \mathbf{M}^{-1} \mathbf{M} (\sigma^2 \mathbf{I}_d + \mathbf{M}^{-1} \mathbf{W}^\top \mathbf{S} \mathbf{W})^{-1} \\ &= \mathbf{S} \mathbf{W} (\sigma^2 \mathbf{I}_d + \mathbf{M}^{-1} \mathbf{W}^\top \mathbf{S} \mathbf{W})^{-1} \end{aligned}$$

where $\mathbf{S} = \frac{1}{N} \sum_{j=1}^N (\hat{\mathbf{x}}_j - \hat{\boldsymbol{\mu}}) (\hat{\mathbf{x}}_j - \hat{\boldsymbol{\mu}})^\top$ has the same form as the usual maximum likelihood estimates of the variance-covariance matrix for the (estimated) sample $\hat{\mathbf{x}}_1, \dots, \hat{\mathbf{x}}_N$ with estimated mean vector $\hat{\boldsymbol{\mu}}$ and $\mathbf{M} = \mathbf{W}^\top \mathbf{W} + \sigma^2 \mathbf{I}_d$.

After substituting $\hat{\mathbf{W}}$ in $\Gamma(\hat{\boldsymbol{\mu}}, \hat{\mathbf{W}}, \sigma^2, \hat{\mathcal{K}}|\mathcal{Y})$ and using Equation (2) in the paper, the estimating equation of σ^2 is

$$\begin{aligned} \frac{\partial \Gamma(\hat{\boldsymbol{\mu}}, \hat{\mathbf{W}}, \sigma^2, \hat{\mathcal{K}}|\mathcal{Y})}{\partial \sigma^2} &= \sum_{j=1}^N -\frac{D}{\sigma^2} - \frac{1}{\sigma^4} \left[\text{tr}[(\hat{\mathbf{x}}_j - \hat{\boldsymbol{\mu}}) (\hat{\mathbf{x}}_j - \hat{\boldsymbol{\mu}})^\top] \right. \\ &\quad \left. - \text{tr}(\hat{\mathbf{W}} \mathbb{E}(\mathbf{Z}_j \mathbf{Z}_j^\top | \hat{\mathbf{x}}_j) \hat{\mathbf{W}}^\top) \right] - \frac{2}{\sigma^4} \left[(\hat{\mathbf{x}}_j - \hat{\boldsymbol{\mu}}) \mathbb{E}(\mathbf{Z}_j^\top | \hat{\mathbf{x}}_j) \hat{\mathbf{W}}^\top \right] = 0, \end{aligned}$$

and by calling $\hat{\mathbf{M}} = \hat{\mathbf{W}}^\top \hat{\mathbf{W}} + \hat{\sigma}^2 \mathbf{I}_d$, we obtain

$$\begin{aligned}
\hat{\sigma}^2 &= \frac{1}{ND} \sum_{j=1}^N \left\{ \text{tr}[(\hat{\mathbf{x}}_j - \hat{\boldsymbol{\mu}})(\hat{\mathbf{x}}_j - \hat{\boldsymbol{\mu}})^\top] - \right. \\
&2(\hat{\mathbf{x}}_j - \hat{\boldsymbol{\mu}}) \mathbb{E}(\mathbf{Z}_j^\top | \hat{\mathbf{x}}_j) \hat{\mathbf{W}}^\top - \left. \text{tr}(\hat{\mathbf{W}} \mathbb{E}(\mathbf{Z}_j \mathbf{Z}_j^\top | \hat{\mathbf{x}}_j)) \hat{\mathbf{W}}^\top \right\} \\
&= \frac{1}{D} \text{tr}[\mathbf{S} - 2\mathbf{S}\hat{\mathbf{W}}\hat{\mathbf{M}}^{-1}\hat{\mathbf{W}}^\top + \hat{\mathbf{W}}(\sigma^2\hat{\mathbf{M}}^{-1} + \hat{\mathbf{M}}^{-1}\hat{\mathbf{W}}^\top\mathbf{S}\hat{\mathbf{W}}\hat{\mathbf{M}}^{-1})\hat{\mathbf{W}}^\top] \\
&= \frac{1}{D} \text{tr}[\mathbf{S}(\mathbf{I} - \hat{\mathbf{W}}\hat{\mathbf{M}}^{-1}\hat{\mathbf{W}}^\top)] \\
&= \frac{1}{D} \text{tr}[\mathbf{S}(\mathbf{I} - \hat{\mathbf{W}}(\hat{\mathbf{W}}^\top\hat{\mathbf{W}} + \hat{\sigma}^2\mathbf{I}_d)^{-1}\hat{\mathbf{W}}^\top)].
\end{aligned}$$

SM-5 Number of Components: Cross-Validation

Determining the optimal number of components in PCA is a well-known challenge, as discussed in Section 2. In this section, we will elaborate on the utilization of a Cross-Validation procedure to address this issue. Let's consider a data matrix \mathbf{X} of dimensions $n \times D$, containing D variables, X_1, X_2, \dots, X_D , which we assume to be mean-centered. Using the Singular Value Decomposition (SVD) of X , we can represent X as:

$$\mathbf{X} = \mathbf{U}\boldsymbol{\Lambda}\mathbf{V}^\top \quad (\text{SM-1})$$

where $\mathbf{U}^\top\mathbf{U} = \mathbf{I}_D$, $\mathbf{V}^\top\mathbf{V} = \mathbf{V}\mathbf{V}^\top = \mathbf{I}_D$ and $\boldsymbol{\Lambda} = (\lambda_1, \dots, \lambda_D)$ with $\lambda_1 \geq \dots \geq \lambda_D \geq 0$. If \mathbf{X} has rank D and all the λ_i ($i = 1, \dots, D$) are distinct, then decomposition (SM-1) is unique apart from corresponding sign changes in \mathbf{U} and \mathbf{V} . If we consider x_{ij} and u_{ij} as the (i, j) -th elements of the matrices \mathbf{X} and \mathbf{U} , respectively, decomposition (SM-1) has its elementwise representation as

$$x_{ij} = \sum_{t=1}^D u_{it}\lambda_tv_{tj}.$$

Hence, according to the PCA, if we consider a lower dimension of m dimensions, the variation in the remaining $(D - m)$ dimensions can be regarded as random noise. We can represent the data with m components as:

$$x_{ij} = \sum_{t=1}^m u_{it}\lambda_tv_{tj} + \epsilon_{ij}.$$

where ϵ_{ij} is a residual term.

To do Cross-Validation, at first, by denoting \mathbf{X}_{-j} as the result of deleting the j -th column and \mathbf{X}_{-i} as the result of deleting the i -th row of \mathbf{X} , there are the following equations:

$$\mathbf{X}_{-i} = \bar{\mathbf{U}}\bar{\mathbf{\Lambda}}\bar{\mathbf{V}}^\top$$

where $\bar{\mathbf{U}} = \bar{u}_{st}$, $\bar{\mathbf{V}} = \bar{v}_{st}$ and $\bar{\mathbf{\Lambda}} = \text{diag}(\bar{\lambda}_1, \dots, \bar{\lambda}_D)$ and

$$\mathbf{X}_{-j} = \tilde{\mathbf{U}}\tilde{\mathbf{\Lambda}}\tilde{\mathbf{V}}^\top$$

with $\tilde{\mathbf{U}} = \tilde{u}_{st}$, $\tilde{\mathbf{V}} = \tilde{v}_{st}$ and $\tilde{\mathbf{\Lambda}} = \text{diag}(\tilde{\lambda}_1, \dots, \tilde{\lambda}_{D-1})$. After that, the predictor can be computed as

$$\hat{x}_{ij}(m) = \sum_{t=1}^m (\tilde{u}_{it} \sqrt{\tilde{\lambda}_t})(\bar{u}_{tj} \sqrt{\bar{\lambda}_t}). \quad (\text{SM-2})$$

Each element on the right-hand side of this equation is derived from the SVD of \mathbf{X} after the removal of either the i -th row or the j -th column. It's important to note that the algorithms developed by Bunch and Nielsen [1978] and Bunch et al. [1978] efficiently compute $\tilde{\mathbf{U}}$, $\tilde{\mathbf{V}}$, $\bar{\mathbf{U}}$, and $\bar{\mathbf{V}}$, which are needed for (SM-2). Finally, based on $\hat{x}_{ij}(m)$ for a given number m of components, we can calculate the average squared discrepancy between the actual and predicted values, defined as:

$$PRESS(m) = \frac{1}{nD} \sum_{i=1}^n \sum_{j=1}^D (\hat{x}_{ij}(m) - x_{ij})^2.$$

Consider fitting components sequentially in (SM-2). Define

$$W_m = \frac{PRESS(m-1) - PRESS(m)}{\mathcal{D}_m} \div \frac{PRESS(m)}{\mathcal{D}_r}$$

In this equation, \mathcal{D}_m stands for the degrees of freedom required to fit the m -th component, and \mathcal{D}_r represents the remaining degrees of freedom after fitting this component. The determination of \mathcal{D}_m involves considering the number of parameters that need to be estimated as well as the constraints applied to the eigenvectors at each stage. It can be demonstrated that $\mathcal{D}_m = n + D - 2m$. Consequently, \mathcal{D}_r can be derived through successive subtraction, given the presence of $(n-1)D$ degrees of freedom in the mean-centered matrix X [Wold, 1978]. Following the guidance of Krzanowski [1983], it is recommended to choose the optimal number of components as the highest value of m for which W_m exceeds 0.9.

SM–6 Further numerical experiments

In this section, we provide additional outputs from the simulation studies. Figures SM–1–SM–3 and Figures SM–4–SM–6 show the frequency of dimension selection when the true dimension is $d = 2$ and $d = 3$, respectively. Each figure corresponds to a different sample size ($N = 50, 100, 500$), and each panel within the figures represents a different value of σ^2 .

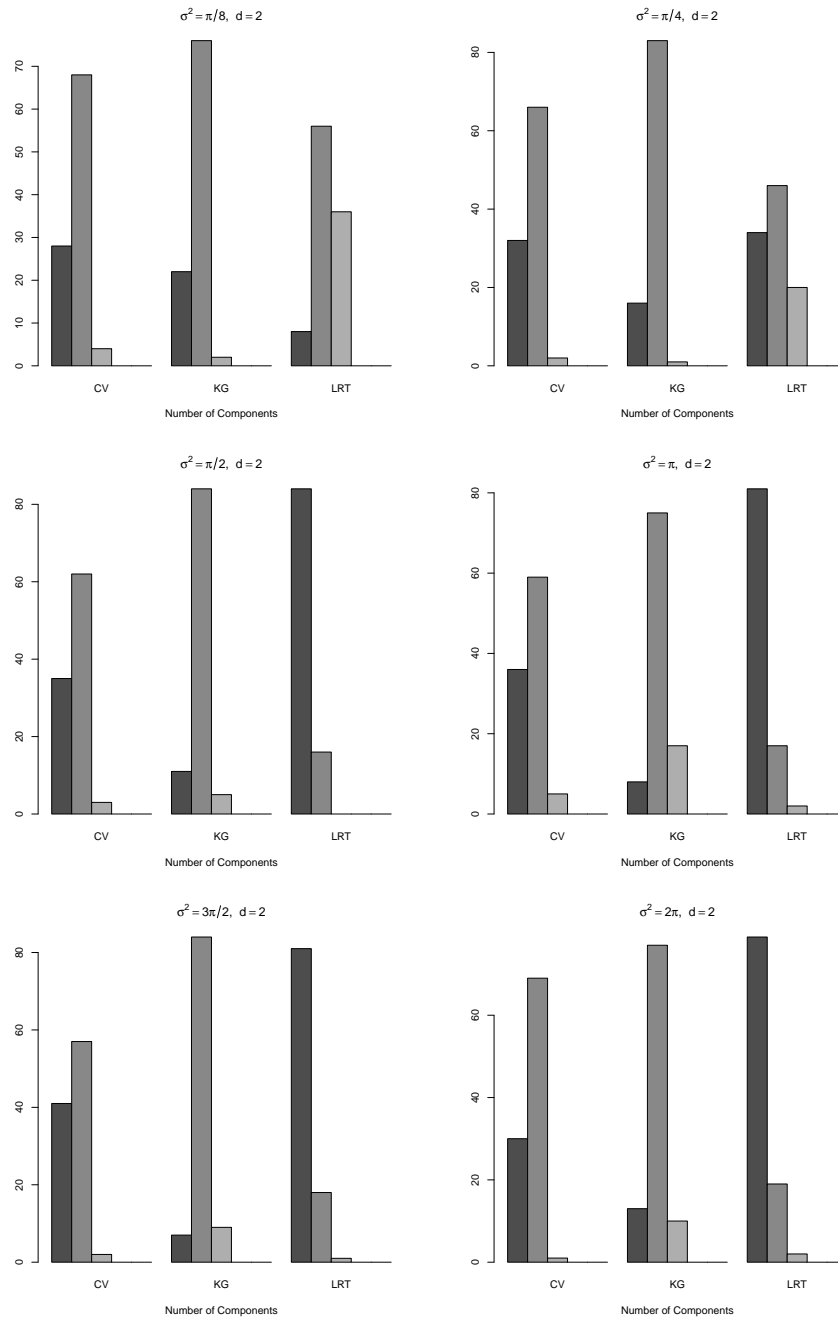


Figure SM-1: Monte Carlo experiment. Frequencies of selection of dimension for CV, KG and LRT. True value is $d = 2$, sample size is 50.

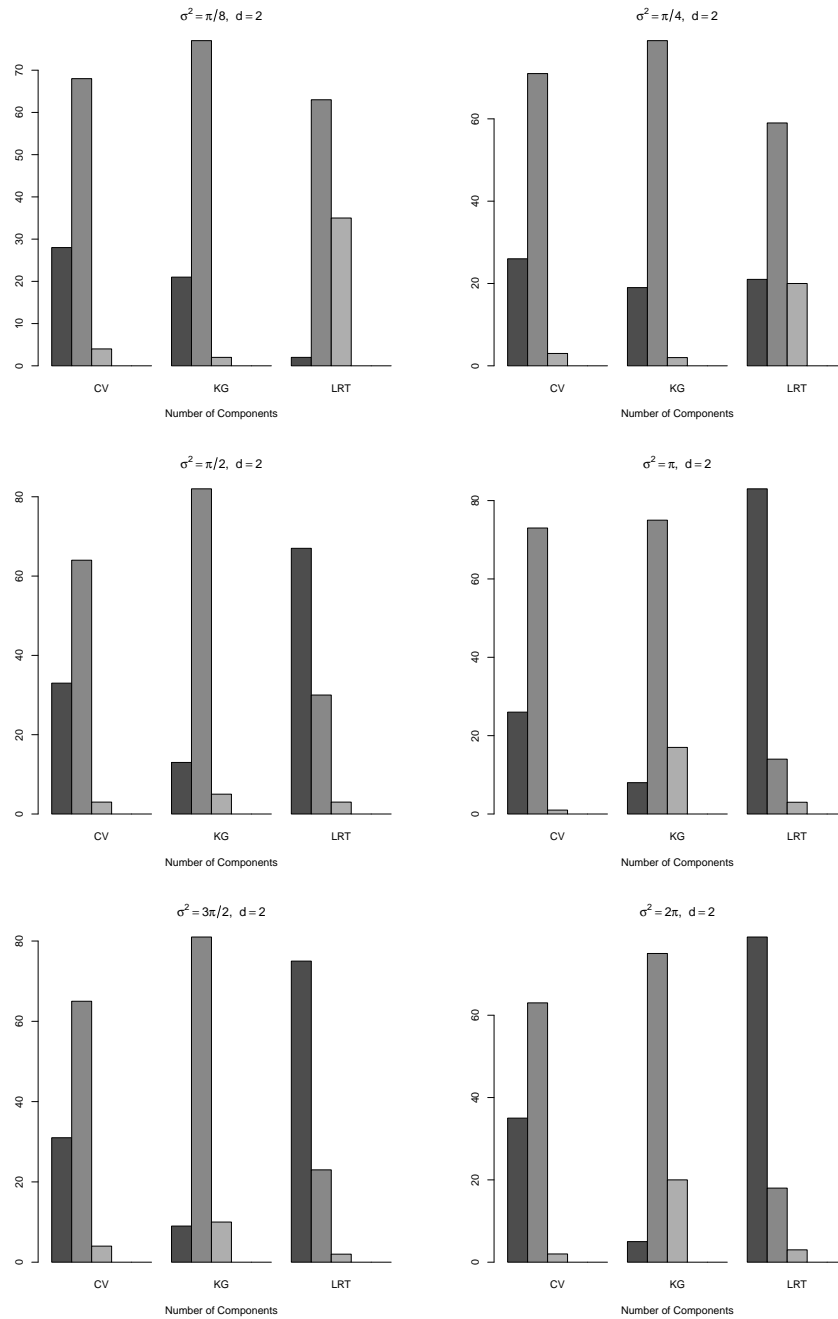


Figure SM-2: Monte Carlo experiment. Frequencies of selection of dimension for CV, KG and LRT. True value is $d = 2$, sample size is 100.

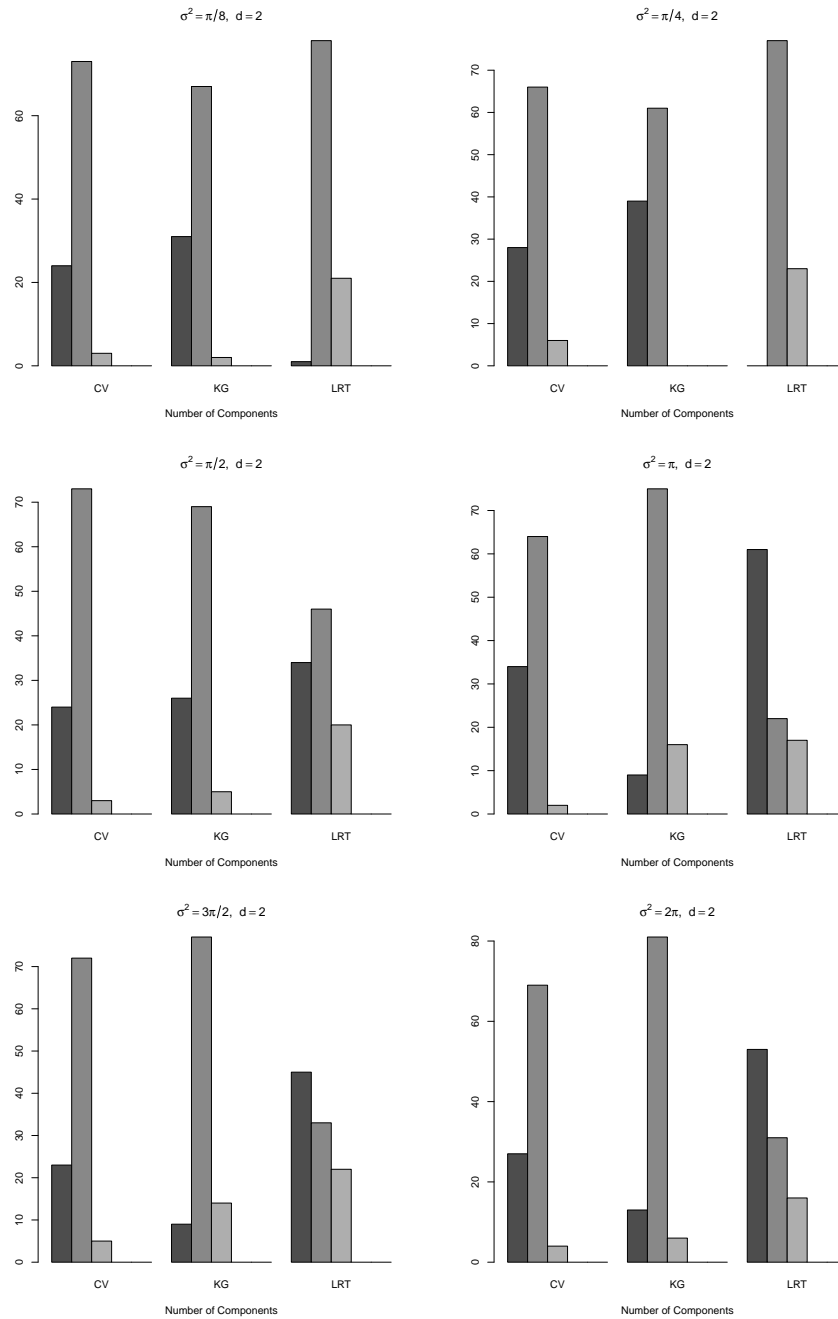


Figure SM-3: Monte Carlo experiment. Frequencies of selection of dimension for CV, KG and LRT. True value is $d = 2$, sample size is 500.

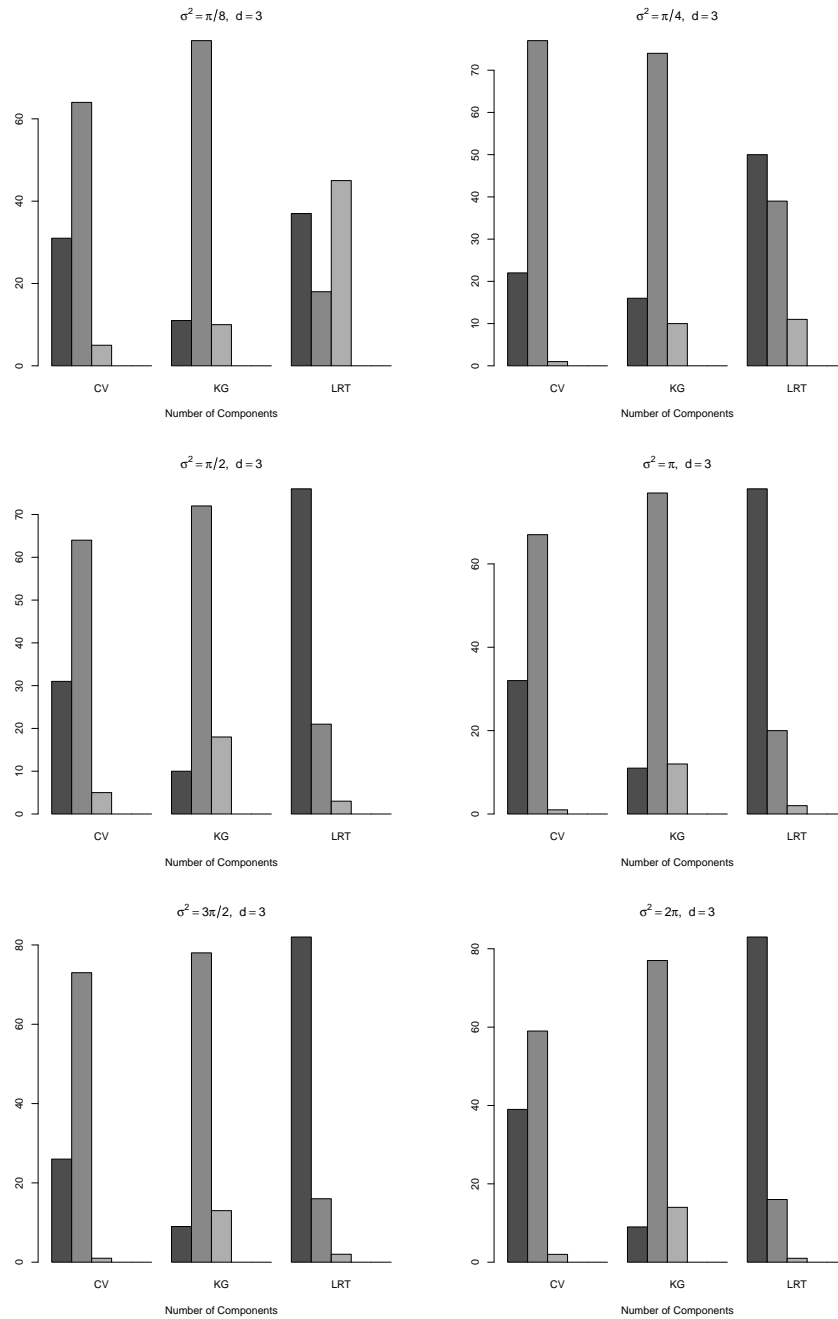


Figure SM-4: Monte Carlo experiment. Frequencies of selection of dimension for CV, KG and LRT. True value is $d = 3$, sample size is 50.

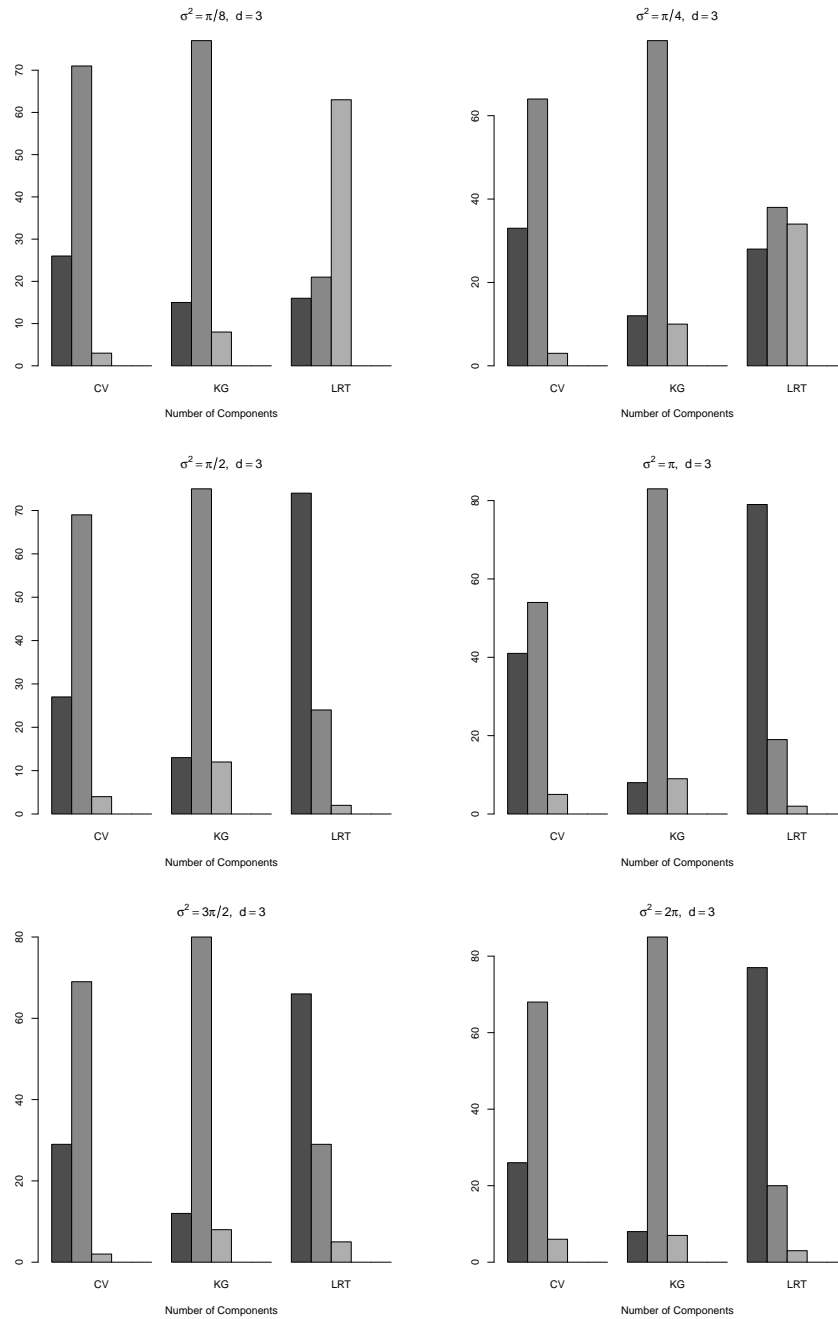


Figure SM-5: Monte Carlo experiment. Frequencies of selection of dimension for CV, KG and LRT. True value is $d = 3$, sample size is 100.

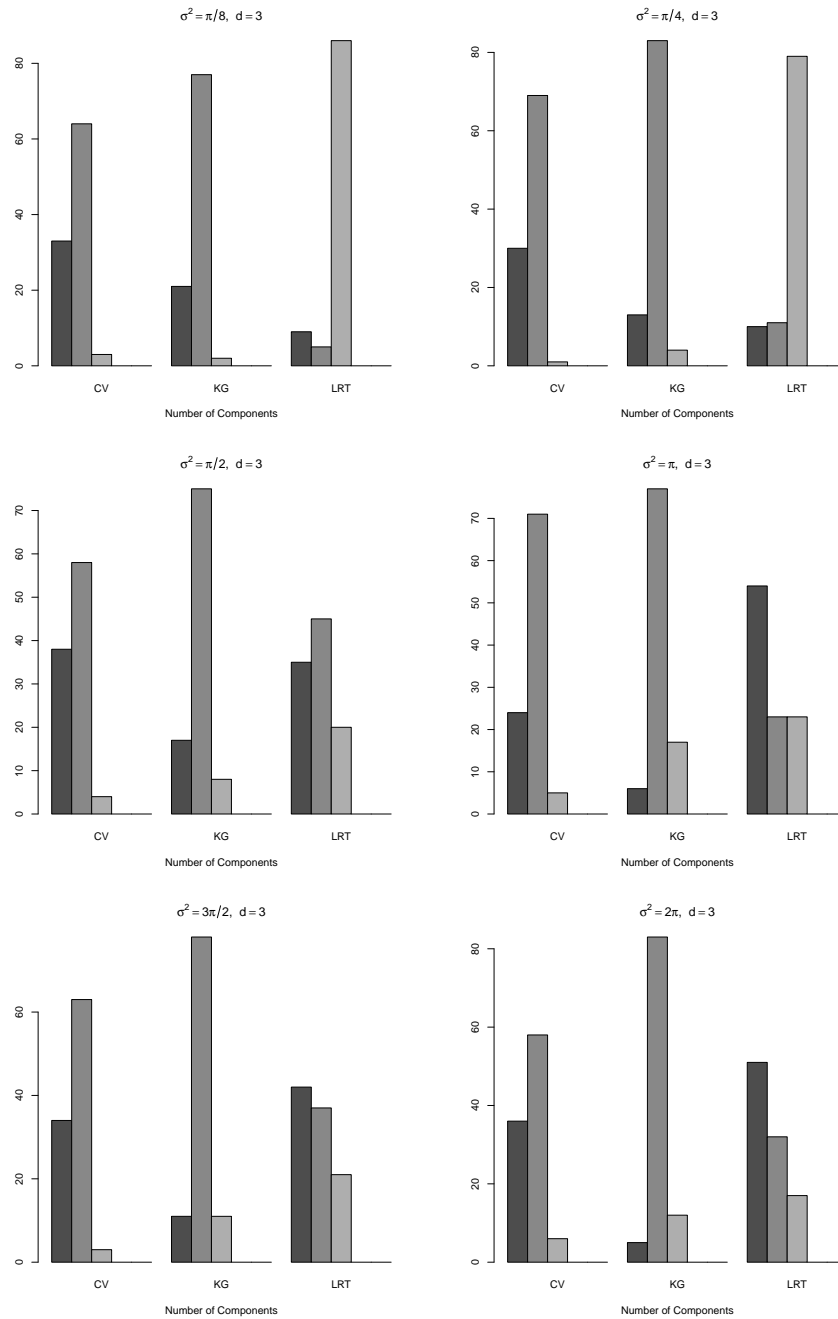


Figure SM-6: Simulation study. Frequencies of selection of dimension for CV, KG, and LRT. The true value is $d = 3$ and the sample size is 500.

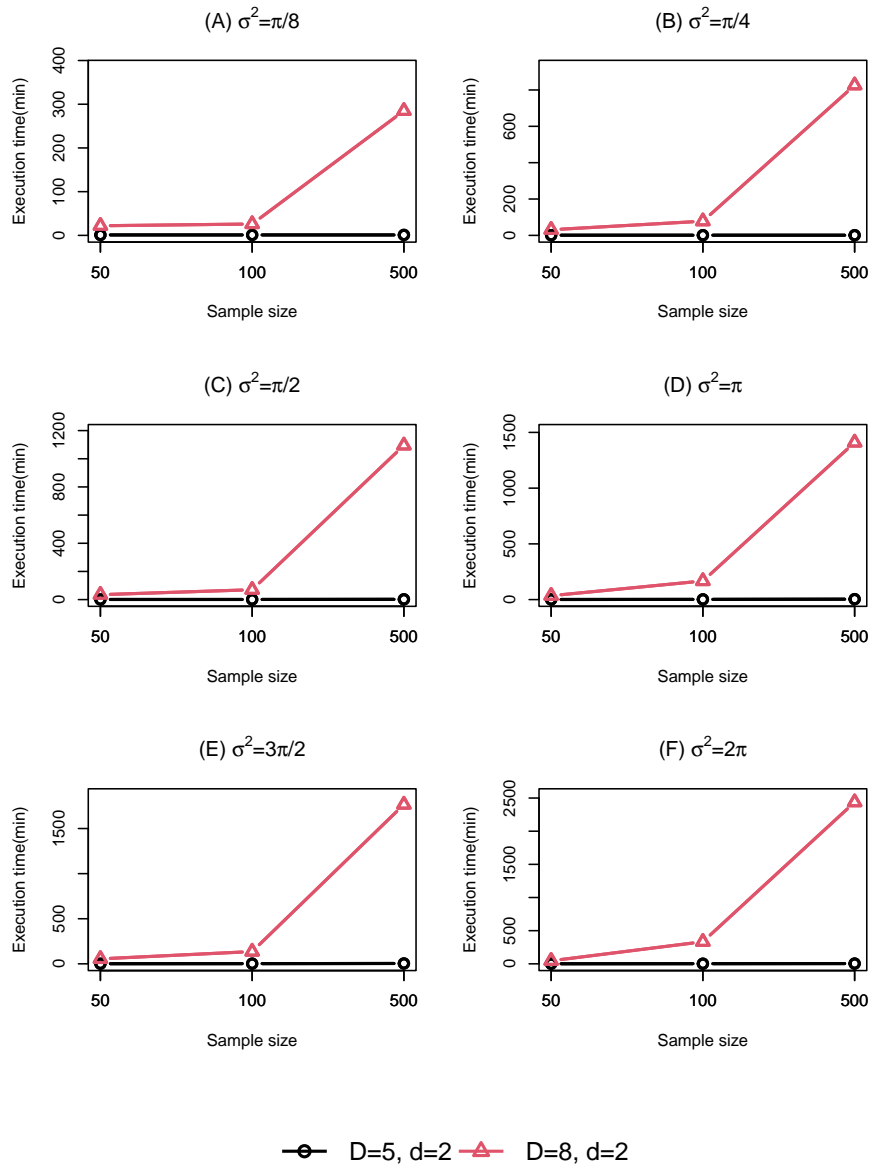


Figure SM-7: Mean execution times for $N = (50, 100, 500)$, and $\sigma^2 = (\pi/8, \pi/4, \pi/2, \pi, 3/2\pi, 2\pi)$ and $d = 2$. Black line: $D = 5$, red line: $D = 8$

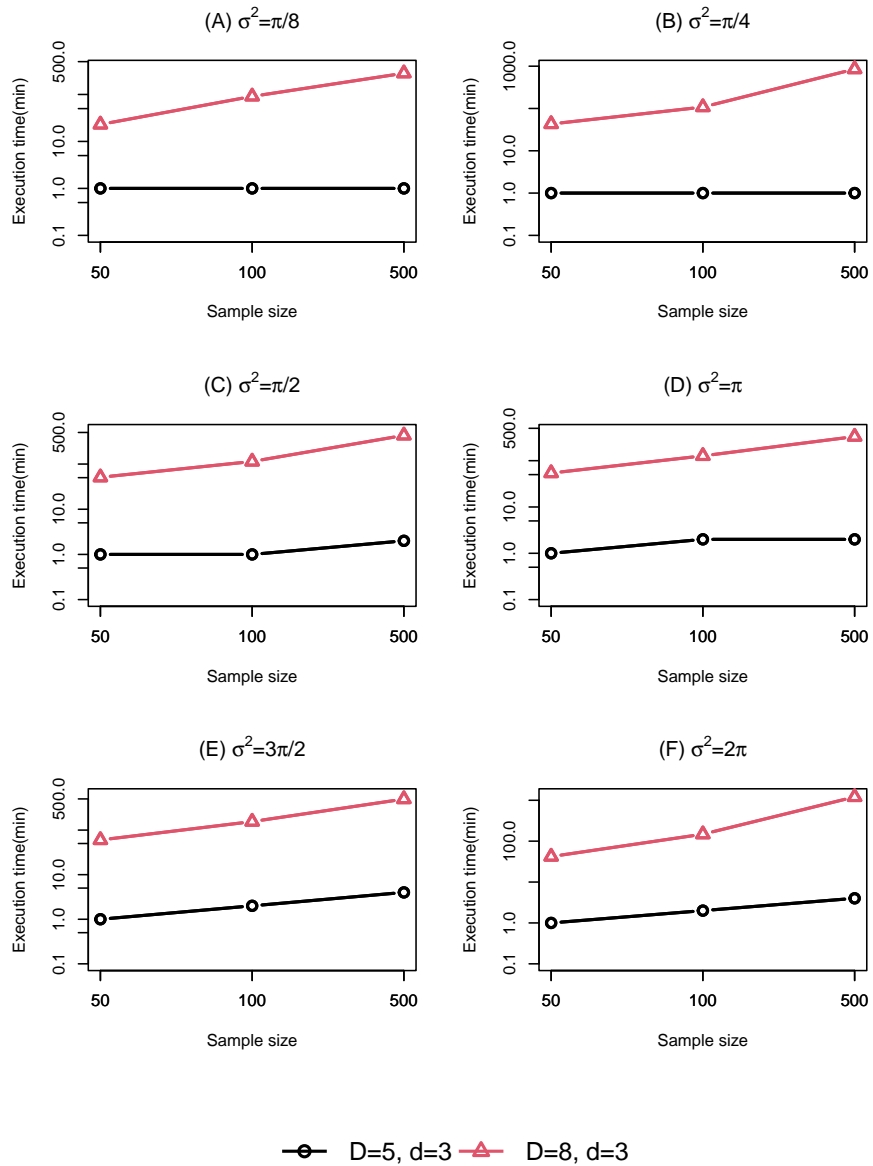


Figure SM-8: Mean execution times for $N = (50, 100, 500)$, and $\sigma^2 = (\pi/8, \pi/4, \pi/2, \pi, 3/2\pi, 2\pi)$ and $d = 3$. Black line: $D = 5$, red line: $D = 8$

SM-7 Large RNA data set

In this section, we present the analysis results from the large RNA (*bigRNA*) dataset. Table SM-1 shows the cumulative percentage of explained variance for each of the 23 clusters after applying the TPPCA algorithm. The number of components was selected based on the LRT, KG, and CV criteria. Consistent with our simulation study findings, the LRT criterion consistently outperformed the others in this real-world scenario.

Cluster #	# points	TPPCA			N. comp.		
		CV	KG	LRT	CV	KG	LRT
1	4917	29.85	83.37	93.74	1	4	5
2	477	51.73	74.53	96.77	1	2	5
3	232	55.21	73.72	95.09	2	3	5
4	211	47.82	76.59	96.72	1	2	5
5	140	69.27	84.29	97.44	1	2	5
6	139	46.19	73.12	97.09	1	2	5
7	139	32.01	77.93	93.66	1	3	5
8	138	83.71	83.71	98.57	2	2	5
9	128	27.53	83.81	92.14	1	4	5
10	122	79.49	66.27	97.90	2	1	5
11	85	57.67	72.89	92.57	2	3	5
12	84	76.75	76.75	96.54	2	2	5
13	79	68.52	83.87	95.51	2	3	5
14	72	71.80	71.80	97.04	2	2	5
15	60	70.99	70.99	96.77	2	2	5
16	60	99.45	98.59	99.75	2	1	3
17	59	68.00	68.00	95.77	2	2	5
18	54	65.62	80.77	80.77	2	3	3
19	52	82.17	82.17	97.71	2	2	5
20	46	96.63	94.11	99.56	2	1	4
21	35	65.49	81.16	95.97	2	3	5
22	33	87.17	87.17	96.61	2	2	4
23	28	64.27	64.27	64.27	2	2	2

Table SM-1: RNA data set. Cumulative of percentage of variance explained by selected components (using CV, KG and LRT) of TPPCA.

References

- A. Agrawal, A. M. Chiu, M. Le, E. Halperin, and S. Sankararaman. Scalable probabilistic pca for large-scale genetic variation data. *PLoS genetics*, 16(5):e1008773, 2020.
- H. Akaike. Factor analysis and AIC. *Psychometrika*, 52:317–332, 1987.
- A. Altis, P. Nguyen, R. Hegger, and G. Stock. Dihedral angles principal component analysis of molecular dynamics simulations. *Journal of Chemical Physics*, 26:244111.1–244111, 2007.
- M.S. Bartlett. Tests of significance in factor analysis. *British Journal of Psychology (Statistics Section)*, 3:77–85, 1950.
- A. Basilevsky. *Statistical Factor Analysis and Related Methods*. Wiley, New York, 1994.
- W. M. Boothby. *An Introduction to Differentiable Manifolds and Riemannian Geometry*. Academic Press, New York, 1986.
- H. Bozdogan. On the frontiers of statistical modeling: An informational approach. *Proceedings of the first US/Japan conference*, 1994.
- G. Brock, V. Pihur, S. Datta, and S. Datta. clvalid: An r package for cluster validation. *Journal of statistical Software*, 25:1–22, 2008.
- J. R. Bunch and C. P. Nielsen. Updating the singular value decomposition. *Numerische Mathematik*, 31:111–129, 1978.
- J. R. Bunch, C. P. Nielsen, and D. C. Sorensen. Rank one modification of the symmetric eigenproblem. *Numerische Mathematik*, 31:31–48, 1978.
- M. Charrad, N. Ghazzali, V. Boiteau, and A. Niknafs. Nbclust: an r package for determining the relevant number of clusters in a data set. *Journal of statistical software*, 61:1–36, 2014.
- M. A. A. Cox and T. F. Cox. Multidimensional scaling. In *Handbook of data visualization*, pages 315–347. Springer, 2008.
- T. F. Cox and M. A. A. Cox. Multidimensional scaling on a sphere. *Communications in Statistics-Theory and Methods*, 20(9):2943–2953, 1991.

- C. M. Duarte and A. M. Pyle. Stepping through an rna structure: a novel approach to conformational analysis. *Journal of molecular biology*, 284(5): 1465–1478, 1998.
- B. Eltzner, S. Huckemann, and K.V. Mardia. Torus principal component analysis with applications to RNA structure. *Annals of Applied Statistics*, 12(2):1332–1359, 2018.
- P. T. Fletcher, C.P. Lu, S. Pizar, and S. C. Joshi. Principal geodesic analysis for the study of nonlinear statistics of shape. *IEEE Trans. Med. Imaging*, 23:995–1005, 2004.
- H. Fotouhi and M. Golalizadeh. Exploring the variability of dna molecules via principal geodesic analysis on the shape space. *Journal of Applied Statistics*, 39(10):2199–2207, 2012.
- H. Fotouhi and M. Golalizadeh. Highly resistant gradient descent algorithm for computing intrinsic mean shape on similarity shape spaces. *Statistical Papers*, 56:391–410, 2015.
- E. García-Portugués and T. Verdebout. sphunif: Uniformity tests on the circle, sphere, and hypersphere. *R package version*, 1(1):8, 2021.
- E. García-Portugués, D. Paindaveine, and T. Verdebout. On optimal tests for rotational symmetry against new classes of hyperspherical distributions. *Journal of the American Statistical Association*, 115(532):1873–1887, 2020.
- L. Guttman. Some necessary conditions for common factor analysis. *Psychometrika*, 19:149–162, 1954.
- T. Hastie and W. Stuetzle. Principal curves. *Journal of American Statistics Association*, 84:502–516, 1989.
- K. Hayashi, P.M. Bentler, and K.H. Yuan. On the likelihood ratio test for the number of factors in exploratory factor analysis. *Structural Equation Modeling*, 14(3):505–526, 2007.
- H. Hotelling. Analysis of a complex of statistical variables into principal components. *Journal of Educational Psychology*, 24:417–441, 1933.
- L. Hubert and P. Arabie. Comparing partitions. *Journal of classification*, 2: 193–218, 1985.

- S. Huckemann and H. Ziezold. Principal component analysis for Riemannian manifolds, with application to triangular shape spaces. *Advances in Applied Probability*, 38:299–319, 2006.
- J. Jackson. *A User's Guide to Principal Component*. John Wiley, New York, 1991.
- I. Jolliffe. *Principal Component Analysis*. Springer, New York, 2002.
- K.G. Jöreskog. Some contributions to maximum likelihood factor analysis. *Psychometrika*, 32:443–482, 1967.
- S. Jung, X. Liu, J.S. Marron, and S. Pizer. Generalized PCA via the backward stepwise approach in image analysis. *Brain, Body and Machine*, 83:111–123, 2010.
- S. Jung, I. L. Dryden, and J.S. Marron. Analysis of principal nested spheres. *Biometrika*, 99:551–568, 2012.
- H.F. Kaiser. The application of electronic computers to factor analysis. *Educational and Psychological Measurement*, 20:141–151, 1960.
- H. Karcher. Riemannian center of mass and mollifier smoothing. *Communications on Pure and Applied Math*, 30(5):509–541, 1977.
- L. Kaufman and P. J. Rousseeuw. *Finding groups in data: an introduction to cluster analysis*. John Wiley & Sons, 2009.
- S. H. Kim, D. Kang, Z. Huo, Y. Park, and G. C. Tseng. Meta-analytic principal component analysis in integrative omics application. *Bioinformatics*, 34(8):1321–1328, 2018.
- K. Koutroumbas and S. Theodoridis. *Pattern recognition*. Academic Press, 2008.
- W. J. Krzanowski. Cross-validatory choice in principal component analysis: Some sampling results. *Journal of Statistical Computation and Simulation*, 18:299–314, 1983.
- W. J. Krzanowski. Cross-validation in principal component analysis. *Biometrics*, 43:575–584, 1987.

- D.N. Lawley and A.E. Maxwell. *Factor Analysis as a Statistical Method*. Elsevier, New York, 1971.
- M. Maadooliat, L. Zhou, S. M. Najibi, X. Gao, and J. Z. Huang. Collective estimation of multiple bivariate density functions with application to angular-sampling-based protein loop modeling. *Journal of the American Statistical Association*, 111(513):43–56, 2016.
- K. V. Mardia, H. Wiechers, B. Eltzner, and S. Huckemann. Principal component analysis and clustering on manifolds. *Journal of Multivariate Analysis*, 188:104862, 2022.
- K.V. Mardia. *Statistics of Directional data*. Academic Press, London, 1972.
- K.V. Mardia, J.T. Kent, and J.M. Bibby. *Multivariate Analysis*. Academic Press, London, 1979.
- M. Moghimbeygi and A. Nodehi. Multinomial principal component logistic regression on shape data. *Journal of Classification*, 39(3):578–599, 2022.
- Y. Mu, P.H. Nguyen, and G. Stock. Energy landscape of a small peptide revealed by dihedral angles principal component analysis. *Proteins*, 58:45, 2005.
- A. Nodehi, M. Golalizadeh, and A. Heydari. Dihedral angles principal geodesic analysis using nonlinear statistics. *Journal of Applied Statistics*, 42:1962–1972, 2015.
- A. Nodehi, M. Golalizadeh, M. Maadooliat, and C. Agostinelli. Estimation of parameters in multivariate wrapped models for data on a p-torus. *Computational Statistics*, 36:193–215, 2021.
- J. Novembre and M. Stephens. Interpreting principal component analyses of spatial population genetic variation. *Nature genetics*, 40(5):646–649, 2008.
- V.M. Panaretos, T. Pham, and Z. Yao. Principal flows. *Journal of the American Statistical Association*, 109:424–436, 2014.
- K. Pearson. On lines and planes of closest fit to systems of points in space. *The London, Edinburgh and Dublin Philosophical Magazine and Journal of Science*, 2:559–572, 1901.

- X. Pennec. Intrinsic statistics on Riemannian manifolds: Basic tools for geometric measurements. *Journal of Mathematics and Imaging Vision*, 25:127–154, 2006.
- A. L. Price, N. J. Patterson, R. M. Plenge, M. E. Weinblatt, N. A. Shadick, and D. Reich. Principal components analysis corrects for stratification in genome-wide association studies. *Nature genetics*, 38(8):904–909, 2006.
- F. Privé, K. Luu, M. G.B. Blum, J. J. McGrath, and B. J. Vilhjálmsón. Efficient toolkit implementing best practices for principal component analysis of population genetic data. *Bioinformatics*, 36(16):4449–4457, 2020.
- L. Riccardi, P. H. Nguyen, and G. Stock. Free-energy landscape of RNA hairpins constructed via dihedral angle principal component analysis. *The Journal of Physical Chemistry B*, 113(52):16660–16668, 2009.
- S. Roweis. EM algorithms for PCA and SPCA. *Advances in Neural Information Processing Systems*, 10:626–632, 1998.
- K. Sargsyan, J. Wright, and C. Lim. Geopca: a new tool for multivariate analysis of dihedral angles based on principal component geodesics. *Nucleic Acids Research*, 40:25, 2012.
- G. Schwarz. Estimating the dimension of a model. *The Annals of Statistics*, 6:461–464, 1978.
- F. Sittel, T. Filk, and G. Stock. Principal component analysis on a torus: Theory and application to protein dynamics. *Journal of Chemical Physics*, 147:244101.1–244101.12, 2017.
- R. Tibshirani, G. Walther, and T. Hastie. Estimating the number of clusters in a data set via the gap statistic. *Journal of the Royal Statistical Society: Series B (Statistical Methodology)*, 63(2):411–423, 2001.
- M.E. Tipping and C.M. Bishop. *Probabilistic Principal Component Analysis*. Neural Computing Research, Aston University, Birmingham, 1997. Technical Report.
- M.E. Tipping and C.M. Bishop. Probabilistic principal component analysis. *Journal of the Royal Statistical Society*, 61:611–622, 1999.

- D. N. Wiseman, N. Samra, M. M. R. Lara, S. C. Penrice, and A. D. Goddard. The novel application of geometric morphometrics with principal component analysis to existing g protein-coupled receptor (gpcr) structures. *Pharmaceuticals*, 14:953, 2021.
- S. Wold. Cross-validatory estimation of the number of components in factor and principal component models. *Technometrics*, 20:397–405, 1978.
- M. Zhang and P.T. Fletcher. *Probabilistic Principal Geodesic Analysis*. In Neural Information Processing Systems (NIPS), 2013. Nevada, United States.
- P. Zouboulouglou, E. García-Portugués, and J.S. Marron. Scaled torus principal component analysis. *Journal of Computational and Graphical Statistics*, 32:1024–1035, 2022.